

# The STAGGER-grid: A grid of 3D stellar atmosphere models

## III. The relation to mixing length convection theory<sup>\*\*\*</sup>

Z. Magic<sup>1,2</sup>, A. Weiss<sup>1</sup> and M. Asplund<sup>2,1</sup>

<sup>1</sup> Max-Planck-Institut für Astrophysik, Karl-Schwarzschild-Str. 1, 85741 Garching, Germany  
 e-mail: magic@mpa-garching.mpg.de

<sup>2</sup> Research School of Astronomy & Astrophysics, ANU Cotter Road, Weston ACT 2611, Australia

Received ...; Accepted...

### ABSTRACT

**Aims.** We investigate the relation between 1D atmosphere models that rely on the mixing length theory and models based on full 3D radiative hydrodynamic (RHD) calculations to describe convection in the envelopes of late-type stars.

**Methods.** The adiabatic entropy value of the deep convection zone,  $s_{\text{bot}}$ , and the entropy jump,  $\Delta s$ , determined from the 3D RHD models, are matched with the mixing length parameter,  $\alpha_{\text{MLT}}$ , from 1D hydrostatic atmosphere models with identical microphysics (opacities and equation-of-state). We also derive the mass mixing length,  $\alpha_m$ , and the vertical correlation length of the vertical velocity,  $C[v_z, v_z]$ , directly from the 3D hydrodynamical simulations of stellar subsurface convection.

**Results.** The calibrated mixing length parameter for the Sun is  $\alpha_{\text{MLT}}^{\odot}(s_{\text{bot}}) = 1.98$ . For different stellar parameters,  $\alpha_{\text{MLT}}$  varies systematically in the range of 1.7 – 2.4. In particular,  $\alpha_{\text{MLT}}$  decreases towards higher effective temperature, lower surface gravity and higher metallicity. We find equivalent results for  $\alpha_{\text{MLT}}^{\odot}(\Delta s)$ . Also, we find a tight correlation between the mixing length parameter and the inverse entropy jump. We derive an analytical expression from the hydrodynamic mean field equations that motivates the relation to the mass mixing length,  $\alpha_m$ , and find that it exhibits qualitatively a similar variation with stellar parameter (between 1.6 and 2.4) with a solar value of  $\alpha_m^{\odot} = 1.83$ . The vertical correlation length scaled with the pressure scale height yields for the Sun 1.71, but displays only a small systematic variation with stellar parameters, the correlation length slightly increasing with  $T_{\text{eff}}$ .

**Conclusions.** We derive mixing length parameters for various stellar parameters that can be used to replace a constant value. Within any convective envelope,  $\alpha_m$  and related quantities vary a lot. Our results will help to replace a constant  $\alpha_{\text{MLT}}$ .

**Key words.** convection – hydrodynamics – stars: atmospheres – stars: evolution – stars: late-type – stars: solar-type

### 1. Introduction

In the past century insights in various fields of physics led to a substantially more accurate interpretation and understanding of the processes taking place in the interior of celestial bodies. With theoretical stellar atmosphere models astronomers can parameterize the conditions on the surface of stars, and additionally with the theory of stellar structure and evolution, they are capable to predict the complex development of stars.

The radiated energy of cool stars, originating from the deeper interior due to nuclear burning in the center, is advected to the surface by convective motions in the envelope, driven by negative buoyancy acceleration. At the thin photospheric transition region the large mean free path of photons allows them to escape into space, and the convective energy flux is released abruptly. To model theoretically this superadiabatic boundary domain of stars is challenging due to the non-linear and non-local nature of turbulent sub-surface convection and radiative transfer, and an analytical solution is a long-standing unresolved issue.

To account for the convective energy transport, Böhm-Vitense (1958) formulated the mixing length theory

(MLT), which was initially proposed by Ludwig Prandtl for the Earths atmosphere in analogy to the concept of the mean free path in the kinetic gas theory. In the framework of MLT, it is assumed that the heat flux is carried by convective elements for a typical distance, before they dissolve instantaneously into the background. This distance is the so-called mixing length,  $l$ , usually expressed in units of the pressure scale height,  $\alpha_{\text{MLT}} = l/H_p$ . The mixing length parameter  $\alpha_{\text{MLT}}$  is a priori unknown, hence it has to be “calibrated”, usually by matching the current radius and luminosity of the Sun by a standard solar model with a single depth-independent  $\alpha_{\text{MLT}}^{\odot}$ . This calibrated value for the Sun is then used for all stellar parameters. It must be recalled that  $\alpha_{\text{MLT}}^{\odot}$ , in fact, corrects for all other shortcomings of the solar model, due to, e.g., deficits in the equation-of-state (EOS), the opacities, or the solar composition. It therefore is no wonder that its numerical value (typically around 1.7 to 1.9; e.g., see Magic et al. 2010) varies with progress in the named aspects and from code to code. In addition, MLT is a local and time-independent theory that contains effectively three additional, free parameters, and assumes symmetry in the up- and downflows, hence also in the vertical and horizontal direction. The actual formulation of MLT can vary slightly too (e.g., see Henyey et al. 1965; Mihalas 1970; Ludwig et al. 1999).

Many attempts have been made to improve MLT, a substantial one being the derivation of a non-local mixing

Send offprint requests to: magic@mpa-garching.mpg.de

\* Appendix is available in electronic form at <http://www.aanda.org>

\*\* Full Table A.1 is available at the CDS via anonymous ftp to cdsarc.u-strasbg.fr (130.79.128.5) or via <http://cdsarc.u-strasbg.fr/viz-bin/qcat?J/A+A/??/?A??>, as well as at [www.stagger-stars.net](http://www.stagger-stars.net).

length theory (Gough 1977; Unno et al. 1985; Deng et al. 2006; Grossman et al. 1993). The standard MLT is a local theory, i.e. the convective energy flux is derived purely from local thermodynamical properties, ignoring thus any non-local properties (e.g. overshooting) of the flow. Usually, the non-local models are derived from the hydrodynamic equations, which are a set of non-linear moment equations including higher order moments. For their solution, closure approximations are considered (e.g. diffusion approximation, anelatic approximations or introducing a diffusion length). Also, further aspects have been studied: the asymmetry of the flow by a two stream MLT model (Nordlund 1976), the anisotropy of the eddies (Canuto 1989), the time-dependence (Xiong et al. 1997) and the depth-dependence of  $\alpha_{\text{MLT}}$  (Schlattl et al. 1997). While standard MLT accounts for only a single eddy size (being  $l$ ), Canuto & Mazzitelli (1991) extended the picture to a larger spectrum of eddy sizes by including the non-local second order moment (Canuto et al. 1996, see also). The original Canuto-Mazzitelli-theory – also known as the *Full Spectrum Turbulence* model – used the distance to the convective region border, as a proxy for the mixing length, a later version (Canuto & Mazzitelli 1992) re-introduced a free parameter resembling  $\alpha_{\text{MLT}}$ .

These approaches are often non-trivial, but so far the standard MLT is still widely in use, and a breakthrough has been absent, despite all the attempts for improvements. In 1D atmosphere modeling, the current procedure is to assume for the mixing length parameter  $\alpha_{\text{MLT}}$  a universal value of 1.5 (Gustafsson et al. 2008; Castelli & Kurucz 2004, see). For full stellar evolution models, the solar “calibration” yields values around  $\sim 1.7 - 1.9$  (Magic et al. 2010, see, e.g.). Since the value of the mixing length parameter sets the convective efficiency and therefore changes the superadiabatic structure of stellar models, an accurate knowledge of  $\alpha_{\text{MLT}}$  for different stellar parameters would be a first step in improving models in that respect. However, besides the Sun, other calibrating objects are rare and data are much less accurate (see Sect. 3.7 for an example), such as binary stars with well determined stellar parameters.

The mixing length parameter can be deduced from multidimensional radiative hydrodynamic (RHD) simulations, where convection emerges from first principles (e.g., see Ludwig et al. 1999). Over the past decades, the computational power has increased and the steady development of 3D RHD simulations of stellar atmospheres has established their undoubted liability by manifold successful comparisons with observations (Nordlund 1982; Steffen et al. 1989; Ludwig et al. 1994; Freytag et al. 1996; Stein & Nordlund 1998; Nordlund & Dravins 1990; Nordlund et al. 2009). The 3D RHD models have demonstrated that the basic picture of MLT is incorrect, namely, the convective bubbles are not present, instead highly asymmetric convective motions are found. Nonetheless, an equivalent mixing length parameter has been calibrated by Ludwig et al. (1999) based on 2D hydrodynamic models by matching the resulting adiabats with 1D MLT models (see Freytag et al. 1999, for the metal-poor cases). They had shown that  $\alpha_{\text{MLT}}$  varies significantly with the stellar parameters (from 1.3 to 1.8), and they also studied the impact of a variable  $\alpha_{\text{MLT}}$  on globular cluster (Freytag & Salaris 1999). Also, Trampedach (2007) applied a grid of 3D atmosphere models with solar metallicity for the calibration of the mixing length parameter (from 1.6 to 2.0), and the so-called mass mixing length (Trampedach & Stein 2011).

In the present work we calibrate the mixing length parameter with a 1D atmosphere code that consistently employs the identical EOS and opacity as used in the 3D RHD simulations

(Sect. 2). We present the resulting mixing length parameter in Sect. 3. We also determine the mass mixing length – the inverse gradient of the vertical mass flux – in Sect. 4, and the vertical correlation length of the vertical velocity (Sect. 5) directly from the 3D atmosphere models. For the former quantity, we derive a relation from the hydrodynamic mean field equations that demonstrates the relation to  $\alpha_{\text{MLT}}$ , which is further substantiated by our numerical results. Finally, we conclude our findings in Sect. 6.

## 2. Theoretical models

### 2.1. 3D atmosphere models

We have computed the STAGGER-grid, a large grid of 3D RHD atmosphere models covering a wide range in stellar parameter space (see Magic et al. 2013a, hereafter Paper I). The 3D atmosphere models are computed with the STAGGER-code, which solves the 3D hydrodynamic equations for conservation of mass, momentum and energy, coupled with a realistic treatment of the radiative transfer. We employ the EOS by Mihalas et al. (1988), and up-to-date continuum and lines opacities (Gustafsson et al. 2008). For the solar chemical abundances, we use the values by Asplund et al. (2009, hereafter AGS09). Our simulations are of the so-called “box-in-a-star” type, i.e. we compute only a small, statistically representative volume that includes typically ten granules. Also, our (shallow) simulations cover only a small fraction of the total depth of the convective envelope. Due to the adiabaticity of the gas in the lower parts of the simulation box, the asymptotic entropy value of the convective zone,  $s_{\text{ad}}$ , is matched by the fixed entropy at the bottom of the simulation domain,  $s_{\text{bot}}$ , which is one of the simulation parameters. The effective temperature is therefore a result in our 3D simulations, and is actually a temporally averaged quantity. In 1D models  $T_{\text{eff}}$  is an actual fixed input value in addition without fluctuations.

We determine the entropy jump,  $\Delta s$ , as the difference between the entropy minimum and the constant entropy value of the adiabatic convection zone with  $\Delta s = s_{\text{min}} - s_{\text{bot}}$ . In Magic et al. (2013b, hereafter Paper II), we studied in detail the differences between mean (3D) models resulting from different reference depth scales. In the present work, we show and discuss only averages on constant geometrical height  $\langle 3D \rangle_z$ , since these fulfill the hydrodynamic equilibrium and extend over the entire vertical depth of the simulations. The STAGGER-grid encompasses  $\sim 220$  models ranging in effective temperature,  $T_{\text{eff}}$ , from 4000 to 7000 K in steps of approximately 500 K (recall that  $T_{\text{eff}}$  is the result of the input quantity  $s_{\text{ad}}$ , and the intended  $T_{\text{eff}}$  grid point values are adjusted within a margin below 100 K). Surface gravity,  $\log g$ , ranges from 1.5 to 5.0 in steps of 0.5 dex, and metallicity,  $[\text{Fe}/\text{H}]$ , from  $-4.0$  to  $+0.5$  in steps of 0.5 and 1.0 dex. We refer the interested reader to Paper I for detailed information on the actual methods for computing the grid models, their global properties and mean stratifications.

### 2.2. 1D atmosphere models

For the STAGGER-grid, a 1D MLT atmosphere code has been developed, which uses exactly the same opacities and EOS as the 3D models (Paper I). Therefore, the chemical compositions are identical. The code uses the MLT formulation by Henyey et al. (1965) (see App. C.1 for details), similar to the MARCS code (Gustafsson et al. 2008). Furthermore, we note that for consistency, the 1D models are computed with exactly the same  $T_{\text{eff}}$  as the 3D models.

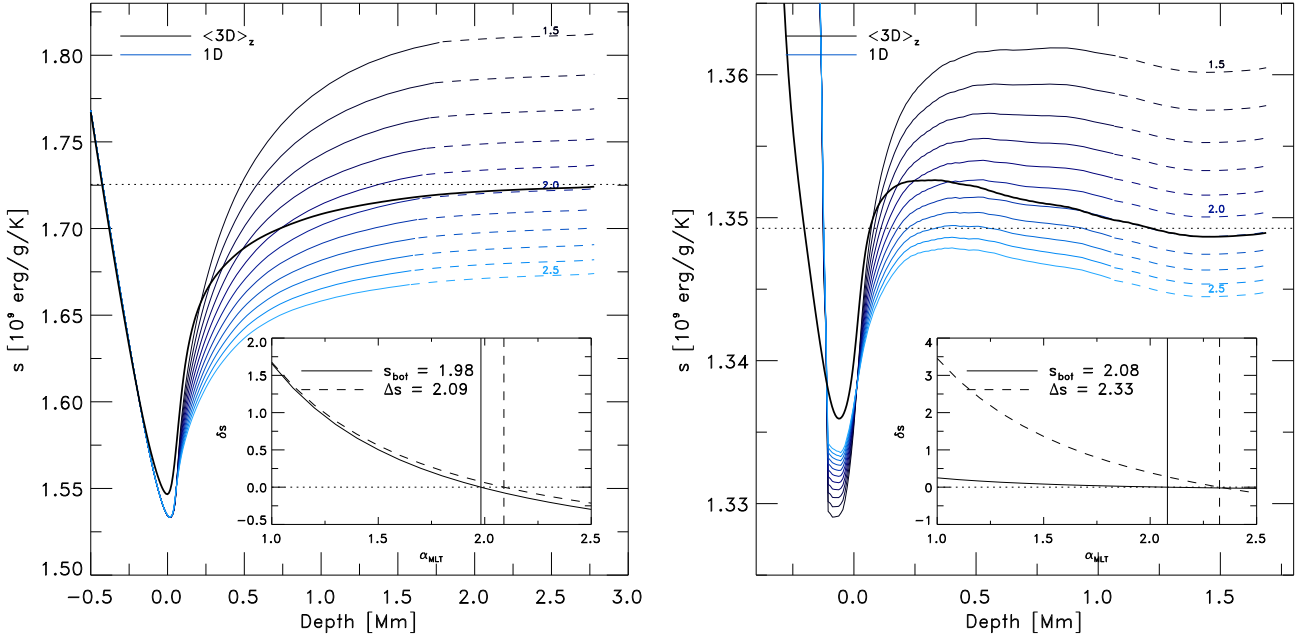


**Fig. 1.** Showing the mean  $\langle 3D \rangle_z$  entropy (black solid line) vs. depth, and 1D models for different mixing length parameters,  $\alpha_{MLT} = 1.5 - 2.5$  (blue lines), for the solar model (left panel) and a metal-poor dwarf with  $[Fe/H] = -2.0$ ,  $T_{eff} = 4500\text{K}$ , and  $\log g = 4.5$  (right panel). We indicate the constant entropy value of the deep adiabatic convection zone,  $s_{bot}$ , in both figures by the horizontal dotted line. In the deeper layers, we extended the 1D models (dashed lines) with the aid of the entropy gradient from the  $\langle 3D \rangle$  models. The calibration of the mixing length parameter  $\alpha_{MLT}$  is illustrated by the smaller insets, which depict the relative differences between the 1D and 3D models ( $\delta s = s_{1D}/s_{3D} - 1$ ) for  $s_{bot}$  (solid) and the entropy jump  $\Delta s$  (dashed). For the solar model the two approaches result in  $\alpha_{MLT} = 1.98$  and  $2.09$ , respectively.

The actual implementation of MLT differs slightly depending on the considered code (e.g. Ludwig et al. 1999). In the standard MLT formulation there are in total four parameters. The mixing length parameter,  $\alpha_{MLT} = l/H_p$ , sets the convective efficiency, while one assumes for the temperature distribution  $y = 3/(4\pi^2) \approx 0.076$ , and for the turbulent viscosity  $\nu = 8$  (see App. C.2 for their discussion). We considered only the mixing length parameter  $\alpha_{MLT}$  for the calibration, while the additional parameters were kept fixed to their default values and the turbulent pressure is entirely neglected.

### 3. Mixing length

#### 3.1. Matching the mixing length parameter

We calibrated  $\alpha_{MLT}$  by matching either the asymptotic entropy value of the deep convection zone,  $s_{bot}$ , or the entropy jump,  $\Delta s$ , from the 1D and 3D models. Subsequently, we refer to these with  $\alpha_{MLT}(s_{bot})$  and  $\alpha_{MLT}(\Delta s)$ , respectively. The value of  $s_{bot}$  is an input parameter in our 3D simulations, and represents the adiabatic entropy of the incoming upflows at the bottom of the box that are replenishing the outflows. The *horizontally and temporally averaged entropy* at the bottom,  $\langle s \rangle_{bot}$ , considers in contrast both the up- and downflows, and is thus slightly lower than  $s_{bot}$  due to the entropy-deficient downflows. However, in our simulations the deeper layers are very close to adiabatic conditions. The entropy contrast at the bottom is extremely small,  $\langle s \rangle_{bot} - s_{bot} \ll 1\%$ .

For the calibration, we computed 1D models with  $\alpha_{MLT}$  from 1.0 to 2.5 in steps of 0.1 and determined  $\alpha_{MLT}$  by minimizing the difference  $\delta s = s_{bot}^{1D} - s_{bot}^{3D}$  or the difference in the entropy jumps  $\Delta s = \Delta s^{1D} - \Delta s^{3D}$ . We remark that some 1D atmosphere models had convergence issues, when extended to the same depth as the

3D models. Therefore, we had to calculate slightly shallower 1D models. However, we extended the 1D entropy stratifications with the entropy gradients of the  $\langle 3D \rangle$  model (see Fig. 1). Tests showed that the missing depth in the 1D entropy run leads to only minor uncertainties in the resulting  $\alpha_{MLT}$ . We fitted the differences,  $\delta s$ , with a second order polynom to get the value of  $\alpha_{MLT}$ . We emphasize that the calibration of  $\alpha_{MLT}$  is more meaningful for identical EOS, and the entropy is consistently computed. For the calibration, we neglected the turbulent pressure in the 1D models entirely (i.e.  $\beta = 0$ ).

In Fig. 1, we illustrate the calibration of the solar model and for a cool metal-poor dwarf with the mean entropy,  $s$ , in the convection zone. For the solar simulation, we determined a mixing length parameter of  $\alpha_{MLT} = 1.98$  and  $2.09$  from matching either the adiabatic entropy value (left panel) or the entropy jump (right panel). Note how  $s$  converges asymptotically against  $s_{bot}$ . Furthermore, it is also evident from Fig. 1, that for a higher  $\alpha_{MLT}$  the adiabat ( $s_{bot}$ ) of the 1D models is decreasing in the convection zone. The entropy minimum of the  $\langle 3D \rangle_z$  on geometrical height is slightly mismatched by the 1D models, a fact, which is reflected by slightly different calibrated  $\alpha_{MLT}(\Delta s)$  values. In the 1D models  $s_{min}$  varies only little for different  $\alpha_{MLT}$ , and the differences,  $\Delta\alpha_{MLT}$ , are between  $\sim 10^{-4}$  and  $10^{-3}$  (cf. also the right panel). Since the entropy jumps are in general much larger than the variation of  $s_{min}$ , their influence is very small, and only for very cool metal-poor models with very small entropy jumps, differences in  $s_{min}$  might influence the calibration slightly (right panel).

We note that we find in general very similar results for  $\alpha_{MLT}$  by employing a 1D envelope code, which solves the stellar structure equations down to the radiative interior by including the same EOS and opacities (Christensen-Dalsgaard 2008). This is in particular true for solar metallicity. The 1D envelope code

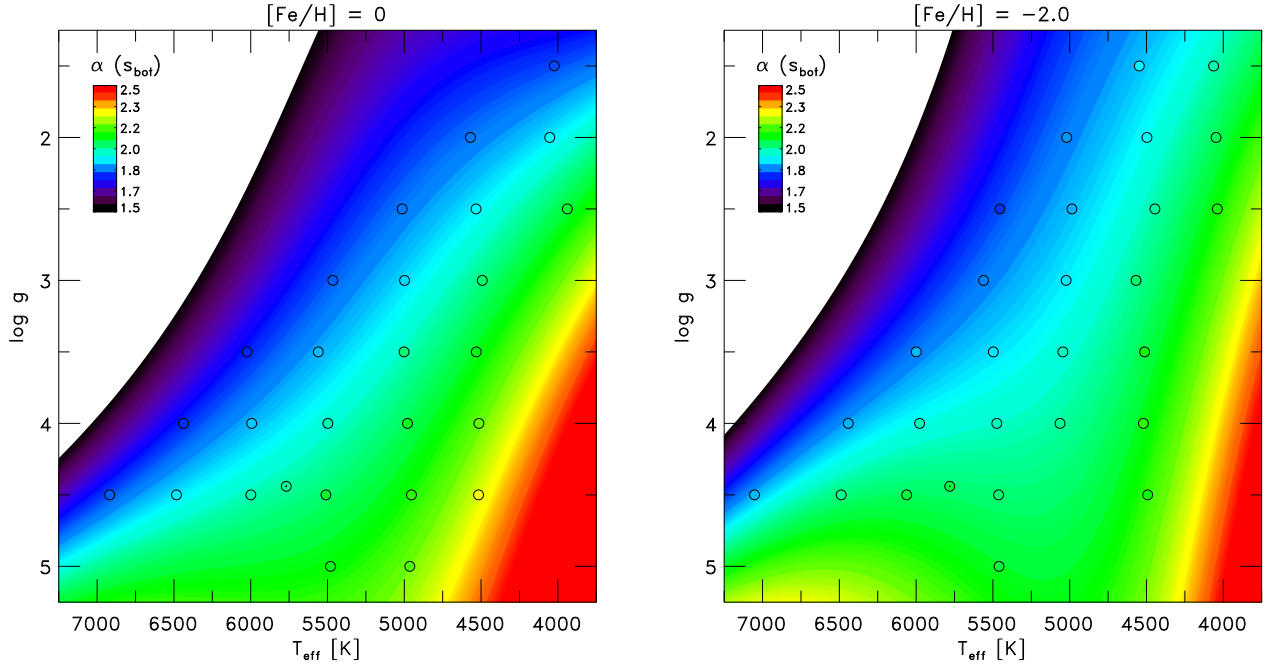


**Fig. 2.** The Kiel-diagram ( $T_{\text{eff}}$  -  $\log g$  diagram) with the mixing length parameter calibrated with the constant entropy value of the adiabatic convection zone,  $\alpha_{\text{MLT}}(s_{\text{bot}})$ , for solar and sub-solar metallicity (left and right panels, respectively). The mixing length is color-coded as indicated and shown with contours derived from functional fits (see App. B), while the circles represent the STAGGER-grid models.

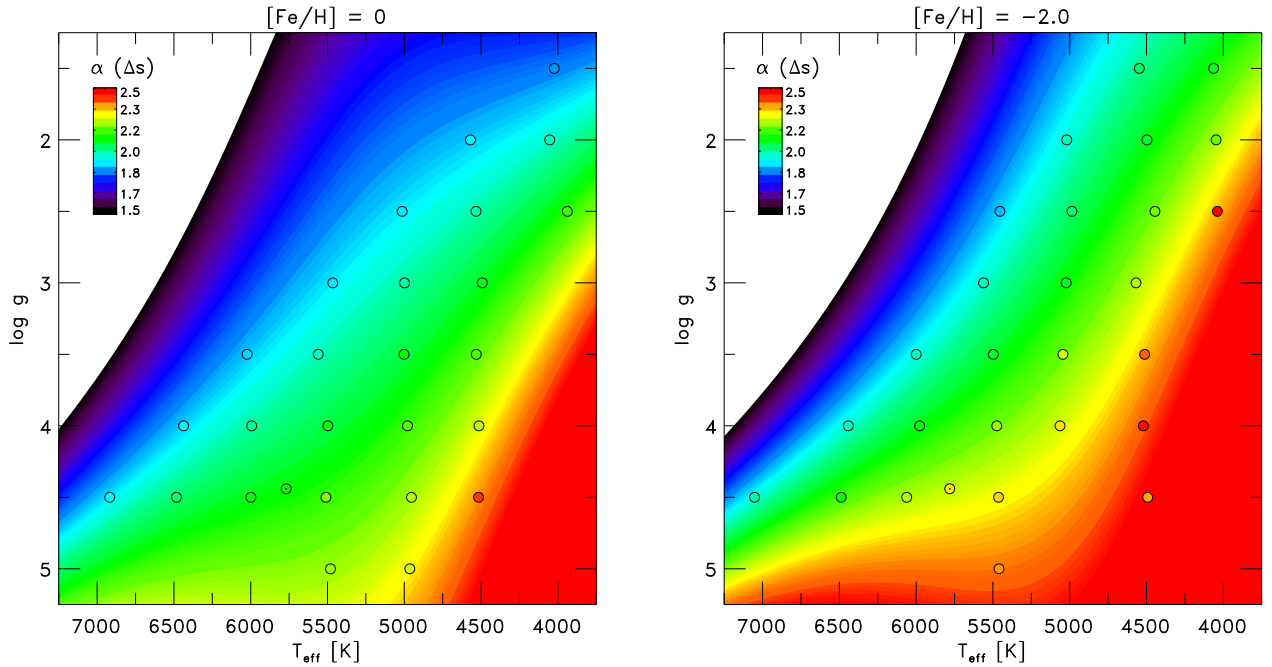


**Fig. 3.** As Fig. 2, but here the mixing length parameter calibrated with the entropy jump  $\alpha_{\text{MLT}}(\Delta s)$  is shown.

relies on an assumed  $T(\tau)$  relation in the (Eddington gray) atmosphere, which obviously influences the thermal stratification at the outer boundary of the convective envelope. In particular, metal-poor 1D convective interior models with a fixed  $T(\tau)$  relation are affected by this, and will return different mixing length parameters. The 1D atmosphere code manages without the need for any  $T(\tau)$  relation, since it solves the radiative transfer by itself. We therefore present and discuss only the mixing length parameters matched by the 1D atmosphere code.

Furthermore, we have performed functional fits for the calibrated mixing length parameters, i.e.  $\alpha_{\text{MLT}} =$

$f(T_{\text{eff}}, \log g, [\text{Fe}/\text{H}])$ , with the same functional basis, as used by Ludwig et al. (1999). For more details see App. B, and the resulting coefficients are provided in Table B.1.

### 3.2. Calibrations with the adiabatic entropy value

In Fig. 2, we show an overview of the variation of the  $\alpha_{\text{MLT}}$  values calibrated with  $s_{\text{bot}}$  for different stellar parameters in the Kiel-diagram, in particular for two illustrating metallicities ( $[\text{Fe}/\text{H}] = 0$  and  $-2$ ). The mixing length parameter varies rather

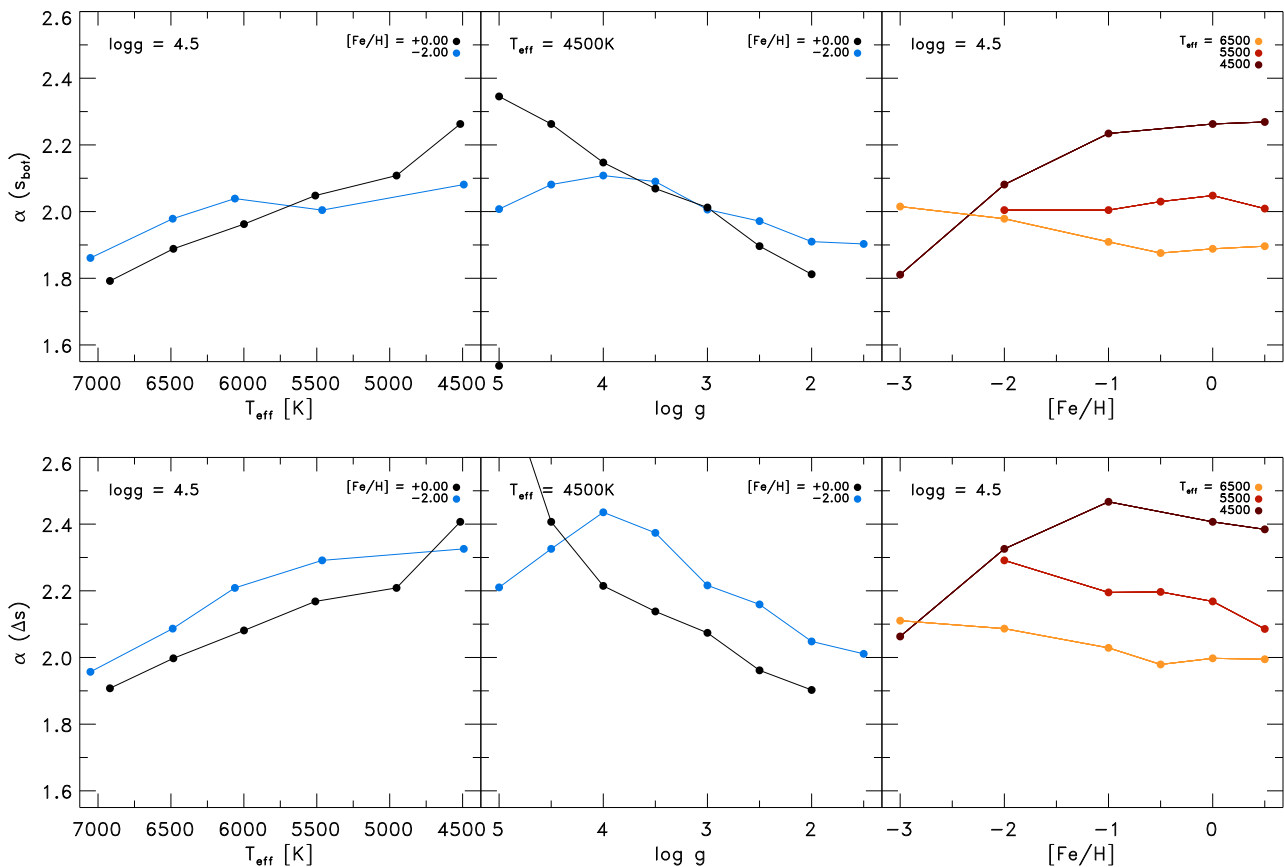


**Fig. 4.** The mixing length parameters illustrating their dependence on the different stellar parameters ( $\alpha_{\text{MLT}}(s_{\text{bot}})$  and  $\alpha_{\text{MLT}}(\Delta s)$  in the top and bottom panel, respectively). We varied one stellar parameter at a time, while the other two are kept fixed (left: effective temperature; middle: surface gravity; right: metallicity). The fixed stellar parameters are indicated and color-coded.

systematically in the range between  $\sim 1.7$  and  $\sim 2.3$ :  $\alpha_{\text{MLT}}$  increases for lower  $T_{\text{eff}}$  and  $[Fe/H]$  and higher  $\log g$  (see also Fig. 4). Some minor deviations (from a linear run) towards cooler  $T_{\text{eff}}$  for metal-poor models can be attributed to the differences in the outer boundary condition of the 1D models. A larger  $\alpha_{\text{MLT}}$  relates to a higher convective efficiency, which implies that a smaller entropy jump is necessary to carry the same convective energy flux. Indeed, we find the entropy jump to increase for higher  $T_{\text{eff}}$ , lower  $\log g$  and higher  $[Fe/H]$  (see Paper I); we find that  $\alpha_{\text{MLT}}$  varies qualitatively inversely to the entropy jump. The mixing length parameter is inversely proportional to the variation of the logarithmic values of the entropy jump, the peak in the entropy contrast and vertical rms-velocity (see Sect. 3.4). This is in agreement with the fact that both the entropy jump and the mixing length parameter are related to the convective efficiency (see Sect. 3.4).

### 3.3. Calibrations with the entropy jump

We also calibrated the mixing length parameter with the 1D MLT atmosphere code by matching the entropy jump  $\Delta s$ . The resulting values are summarized for two metallicities in Fig. 3, showing a similar behavior as the results of the previous section (see also Fig. 4). We find that the  $\alpha_{\text{MLT}}$  values based on  $\Delta s$  are systematically larger by  $\sim 0.1$  (between  $\sim 1.8$  and  $\sim 2.4$ ) than the values based on  $s_{\text{bot}}$  (Fig. 5), but the range in  $\alpha_{\text{MLT}}(\Delta s)$  is with  $\Delta\alpha_{\text{MLT}} \approx 0.6$  very similar to that for  $\alpha_{\text{MLT}}(s_{\text{bot}})$ . The differences arise from the minimum of the entropy  $s_{\text{min}}$  around the optical

surface, which is lower for the 1D models compared to the 3D model (see Fig. 1), therefore leading to larger mixing length parameters. The metal-poor simulations exhibit larger deviations between  $\alpha_{\text{MLT}}(\Delta s)$  and  $\alpha_{\text{MLT}}(s_{\text{bot}})$ , since the boundary effect, induced by the differences in  $\Delta s$ , is increasing for lower  $[Fe/H]$ . We note that the entropy jump is a relative value, and consequently the matching is less prone to outer boundary effects.

### 3.4. Comparison with global properties

We searched for systematic correlations between the mixing length parameter and mean thermodynamic properties. The inverse of the entropy jump correlates well with  $\alpha_{\text{MLT}}$ . In Fig. 6 we demonstrate this by comparing the mixing length parameter  $\alpha_{\text{MLT}}(\Delta s)$  with the logarithm of the inverse of the entropy jump. Convection is driven by radiative cooling in the surface layers. The entropy jump results from the radiative losses at the optical surface, therefore, the correlation of  $\alpha_{\text{MLT}}$  roots in the interplay of the opacity,  $\kappa_\lambda$ , radiative cooling rates,  $q_{\text{rad}}$ , and vertical velocity,  $v_{z,\text{rms}}$ . The vertical velocity results from buoyancy forces,  $f_b = g\Delta\rho$ , acting on the overturning, overdense flows at the optical surface. Hence, a larger entropy jump will entail larger contrast in the entropy and density ( $\delta s_{\text{rms}}$  and  $\delta\rho_{\text{rms}}$ ), which will induce a larger downward acceleration. We illustrate this in Fig. 7, where the peak values for  $\delta s_{\text{rms}}$  and  $\delta\rho_{\text{rms}}$  in the superadiabatic region are plotted against the peak vertical rms-velocity. Evidently, the entropy and density contrast correlate well with the vertical velocity, and this is the underlying reason for the tight

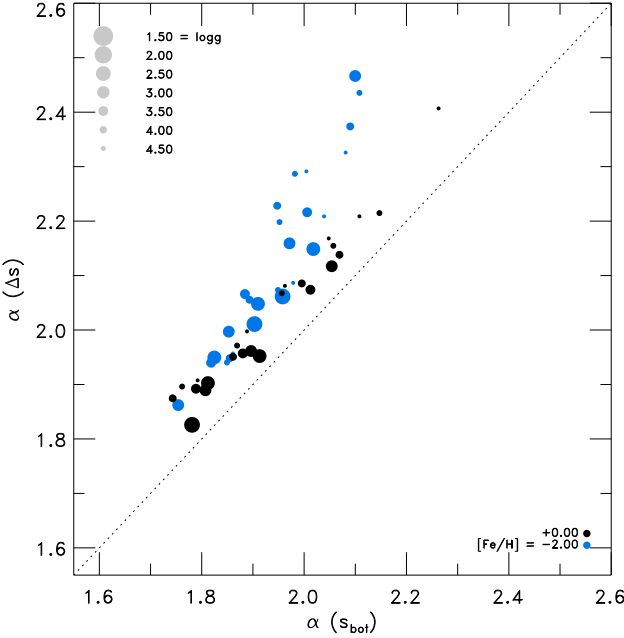


**Fig. 5.** Comparison of the mixing length parameter calibrated with the entropy jump,  $\alpha_{\text{MLT}}(\Delta s)$ , and the constant entropy value of the adiabatic convection zone,  $\alpha_{\text{MLT}}(s_{\text{bot}})$ , for different stellar parameters.

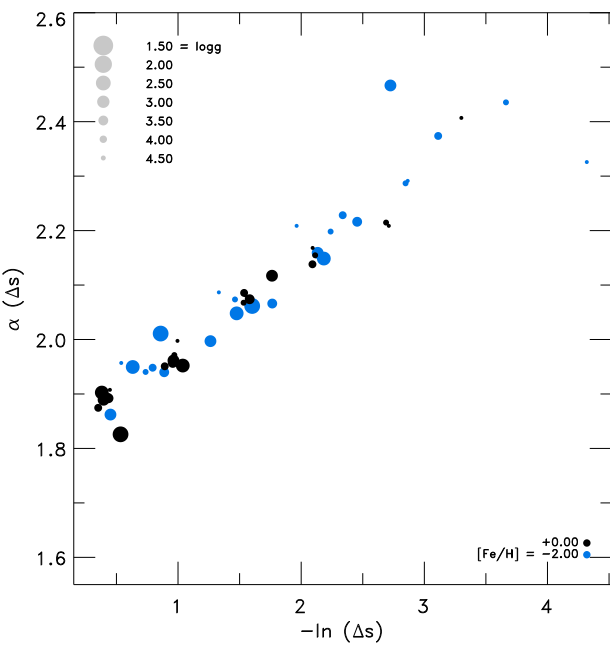


**Fig. 6.** Comparison between the mixing length parameter calibrated with the entropy jump,  $\alpha_{\text{MLT}}(\Delta s)$ , and the logarithm of the inverse of the entropy jump,  $-\ln(\Delta s)$ , for different stellar parameters.

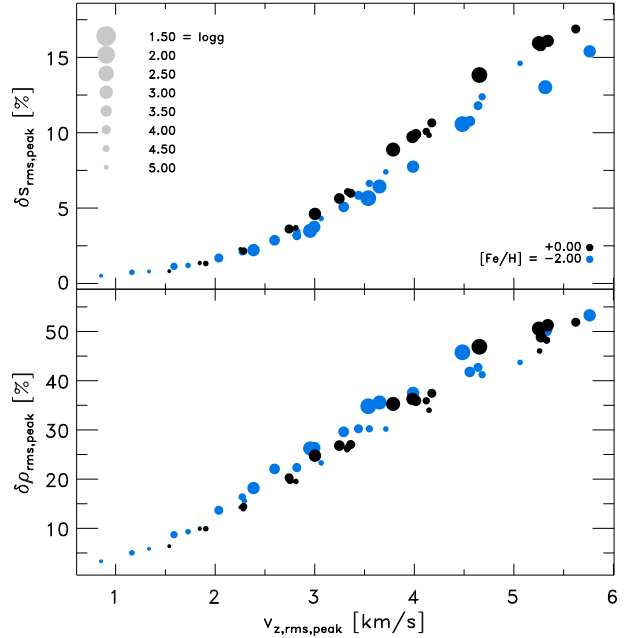


**Fig. 7.** The maximum contrast of the entropy and density compared to the maximum vertical rms-velocity (top and bottom panel, respectively) for different stellar parameters.

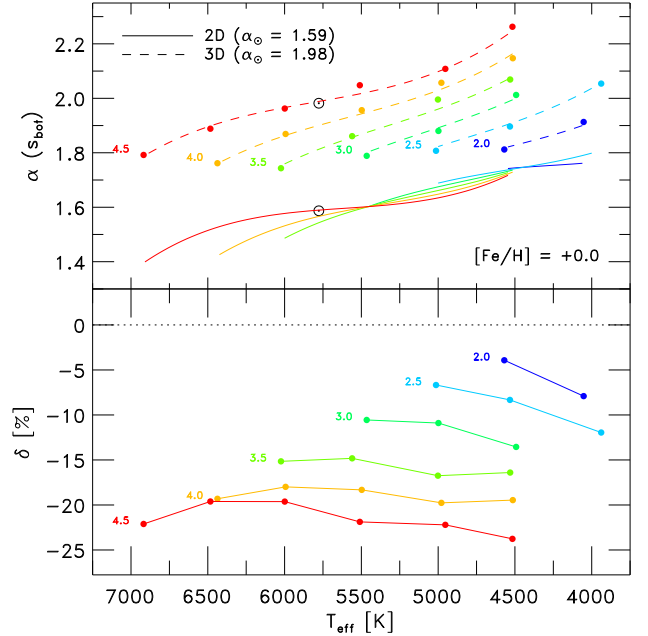


**Fig. 8.** *Top panel:* calibration of  $\alpha_{\text{MLT}}$  with 2D (Ludwig et al. 1999) and 3D simulations in comparison (solid and dashed lines, respectively). The surface gravity is indicated and color-coded. The solar values are indicated. *Bottom panel:* relative differences ( $\delta = 2\text{D}/3\text{D} - 1$ ).

### 3.5. Comparison with 2D calibrations

We compare the differences between our inferred mixing length parameters with those of Ludwig et al. (1999) based on similar, but 2D hydrodynamical surface convection simulations. Also, they matched the resulting 2D-based  $s_{\text{bot}}$  by varying  $\alpha_{\text{MLT}}$  of a 1D envelope code that uses the same EOS and opacity. However, these are not identical to those used by us, and there are

(inverse) correlation between mixing length parameter and entropy jump. In Paper I we have already discussed the correlation of the entropy jump with the peak vertical velocity and the density at the same location, and we deduced the reason for this in the convective energy flux, which essentially contains these quantities.

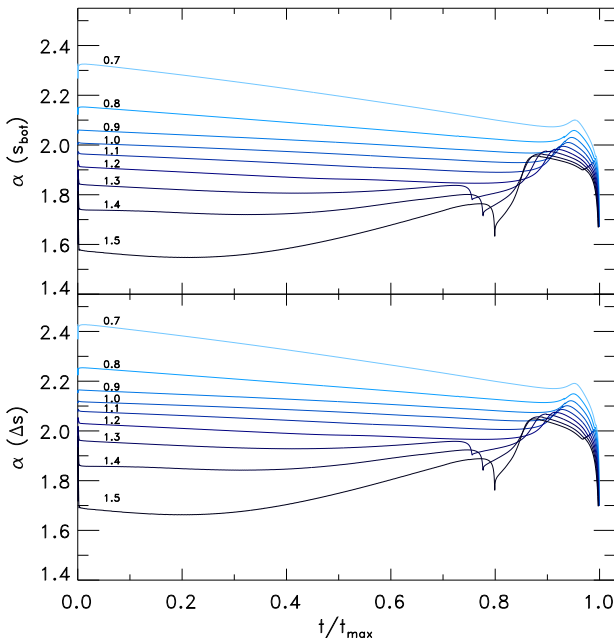


**Fig. 9.** The mixing length parameter along stellar evolutionary tracks with solar metallicity against the normalized age for the masses from  $0.7$  to  $1.5 M_{\odot}$  (indicated). The tracks are derived from the functional fits  $f(T_{\text{eff}}, \log g)$  of  $\alpha_{\text{MLT}}$ -calibrations with  $s_{\text{bot}}$  and  $\Delta s$  (top and bottom panel, respectively) and all tracks end on the RGB when  $\log g = 1$ .

further differences in the models, such as, most importantly, the solar composition. Therefore, these facts should be kept in mind, when interpreting the comparison.

We also remark that Ludwig et al. (1999) derived  $T(\tau)$ -relations from the 2D models, and used them for the 1D models as boundary conditions to render the entropy minimum of the 2D simulations more closely. In Paper I we noticed that  $s_{\text{bot}}$  resulting from the STAGGER-grid is very similar to values from the 2D grid, while the entropy jump  $\Delta s$  exhibits slight differences.

In Fig. 8 we show the calibrated mixing length parameter from both studies in comparison. The results of Ludwig et al. (1999) also show a clear  $T_{\text{eff}}$ -dependence, while surface gravity has only very little influence on  $\alpha_{\text{MLT}}$ . While the 3D-calibrated mixing length parameter decreases with lower surface gravity, its 2D equivalent is moderately increasing. Their solar mixing length parameter is  $\alpha_{\text{MLT}} = 1.59$ , which is lower by 0.39 ( $\sim 20\%$ ) compared to our mixing length parameter, but comparable to the solar model value of that time, as is ours for the present generation of solar models. The  $\alpha_{\text{MLT}}$  values for dwarf models ( $\log g = 4.5$ ) are in general around 20% lower than in our case. Towards giants the difference is diminishing, since the 3D values are decreasing with  $\log g$ . In the case of 3D convection simulations, it is known that convection is more efficient in comparison to the 2D case. Therefore, the mixing length parameters derived from the 3D models are in general systematically larger. Taking into account the aforementioned “model generation effect”, the comparison is, with the exception of the discrepant  $\log g$ -dependence, quite satisfactory.

### 3.6. Impact on stellar evolutionary tracks

When one considers the variation of  $\alpha_{\text{MLT}}$  along typical stellar evolutionary tracks,  $\alpha_{\text{MLT}}$  ranges from 1.6 to 2.4 from higher to lower mass (see Fig. 9), and deviates by up to  $\pm 20\%$  from the

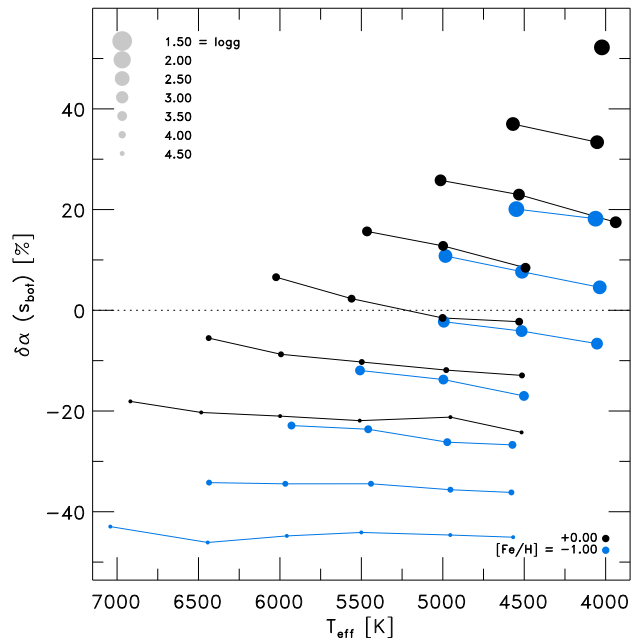


**Fig. 10.** Relative differences between the the mixing length parameter derived from observations and our 3D RHD models for different stellar parameters.

solar value ( $\alpha_{\text{MLT}}^{\odot}$ ). Note that in that figure we show  $\alpha_{\text{MLT}}$  along tracks calculated with a constant value of the mixing length parameter (1.78) obtained from the usual solar model calibration (see Magic et al. 2010). The figure is therefore not showing the actual, self-consistent changes in  $\alpha_{\text{MLT}}$  along the evolution, however, significant differences are hardly to be expected. During the main-sequence evolution  $\alpha_{\text{MLT}}$  varies only little and is almost constant, in particular for the lower masses without a convective core. The variable mixing length parameter has a larger influence during later evolutionary stages, the TO and the RGB ascent;  $\alpha_{\text{MLT}}$  increases first towards values around  $\sim 1.9 - 2.1$ , and then drops sharply down to values of  $\sim 1.7$  for all masses, which is the consequence of the narrow range in red giant temperature and surface gravity.

The mixing length parameter not only determines  $T_{\text{eff}}$  of the stellar models, but also influences the adiabatic stratification of the 1D models in the deeper convection zone. In particular, for a larger  $\alpha_{\text{MLT}}$  the lower boundary of the convection zone is located deeper in the interior. Therefore, for stars with lower (higher) masses, a variable mixing length parameter with stellar parameter will increase (decrease) the depth of the convection zone. As a consequence one can expect that the convective mixing will be enhanced (reduced) for less (more) massive stars in stellar evolutionary calculations. This may influence, for example, the depletion and burning of Li in low-mass stars.

### 3.7. Comparison with observations

Observations provide an opportunity to constrain free parameters in theoretical models. Bonaca et al. (2012) attempted to calibrate the mixing length parameter parameter from Kepler-observations of dwarfs and sub-giants (90 stars). Employing the usual scaling relations for the frequency of the maximal oscillation mode power,  $\nu_{\text{max}}$ , and the large frequency separation,  $\Delta\nu$  (see, for example, Huber et al. 2011), in connection with  $T_{\text{eff}}$  and  $[\text{Fe}/\text{H}]$  from spectroscopic observations, they estimate mass

and radius of the observed objects. Then, from a grid of stellar evolutionary tracks computed with different  $\alpha_{\text{MLT}}$  values, they selected the one matching the inferred stellar parameters.

Bonaca et al. (2012) derived an average mixing length parameter of 1.60 from the observations, being in general lower than their solar-calibrated value with 1.69, which resulted from the 1D models without the comparison with observations. We compare the (linear) functional fit of  $\alpha_{\text{MLT}}$  derived in Bonaca et al. (2012), with stellar parameters to our own results in Fig. 10. We compare the calibration resulting from their complete data set. They also derive a fit for a subset of dwarfs, which, however, is quite restricted in the range of stellar parameters and quite different from the fit for the full sample. Their determined solar mixing length parameter is  $\alpha_{\text{MLT}}^{\odot} = 1.59$ , which is 20% smaller than our result of 1.98. However, we remark that differences between our and their EOS and opacity will have an important impact on  $\alpha_{\text{MLT}}$ , therefore, the comparison between absolute values of  $\alpha_{\text{MLT}}$  are limited. Interestingly, the variation with  $T_{\text{eff}}$  for a given  $\log g$  and  $[\text{Fe}/\text{H}]$  is rather similar apart from an almost constant offset. For different  $\log g$  and  $[\text{Fe}/\text{H}]$ , we find significant systematical differences (see Fig. 10). The values for dwarfs are in general smaller by up to  $\sim 20 - 40\%$  depending on gravity and metallicity, while the giants are greater by the similar amount. The comparison is made more difficult by the fact that even the full sample of Bonaca et al. (2012) is rather limited in  $\log g$ , and biased towards dwarfs. Additionally, the input physics (EOS and opacity) of their models deviates from ours. The authors themselves mention the absence of strong correlations with  $\log g$ , their restricted range in  $[\text{Fe}/\text{H}]$ , the discrepancies to the results by Ludwig et al. (1999) and Trampedach (2007), and the fact that  $\alpha_{\text{MLT}}$  effectively compensates for everything else that influences  $T_{\text{eff}}$ .

Our mixing length parameters differ also significantly from the spectroscopical findings by Fuhrmann et al. (1993), who concluded that one would need an  $\alpha_{\text{MLT}}$  with very low values with  $\sim 0.5$ , in order to properly fit hydrogen lines for various stars with the resulting temperature stratifications. This, however, can be explained completely by the fact that here only the outermost convective layers are traced, which are not tested with our method for inferring  $\alpha_{\text{MLT}}$  from the adiabatic structure at the bottom of the convection zone, and that the mixing length parameter is indeed depth-dependent (see Sect. 4.2). This was already verified by Schlattl et al. (1997).

## 4. Mass mixing length

### 4.1. Deriving the mass mixing length

In the following, we denote the temporal and spatial averaged thermodynamic quantities with  $\langle \dots \rangle$ , which depict only the  $z$ -dependence. Then, the momentum equation for a stationary system yields

$$\partial_z (\langle p_{\text{th}} \rangle + \langle \rho v_z^2 \rangle) = \langle \rho \rangle g.$$

This equation states that a given mass stratification ( $\rho g$ ) has to be supported by the joint thermodynamic ( $p_{\text{th}}$ ) and turbulent pressure ( $p_{\text{turb}} = \rho v_z^2$ ) forces, in order to sustain equilibrium. Since the vertical velocity,  $v_z$ , appears here, we solve for the latter and get

$$\langle v_z \rangle = \sqrt{\frac{g - \langle p_{\text{th}} \rangle / \langle \rho \rangle}{\partial_z \ln \langle \rho \rangle + 2 \partial_z \ln \langle v_z \rangle}}.$$

Then, similar to the temperature gradient,  $\nabla = d \ln \langle T \rangle / d \ln \langle p_{\text{tot}} \rangle$ , we introduce the notation for the gradient for a value  $X$ , however, instead of the total pressure it is scaled by the thermodynamic pressure scale height,

$$\nabla_X = \partial_z \ln \langle X \rangle / \partial_z \ln \langle p_{\text{th}} \rangle,$$

and we can rewrite the vertical velocity to

$$\langle v_z \rangle = \sqrt{\frac{g / \partial_z \ln \langle p_{\text{th}} \rangle - \langle p_{\text{th}} \rangle / \langle \rho \rangle}{\nabla_{\rho} + 2 \nabla_{v_z}}}.$$
 (1)

This analytical exact equation depicts the correlation of the vertical velocity with the gravity and pressure stratification, as well as the gradient of the density and the gradient of the vertical velocity itself in the hydrodynamic equilibrium. Now, we consider the gradient of the absolute vertical mass flux,  $\langle j_z \rangle = \langle \rho v_z \rangle$ , for the up- or downflows (due to conservation of mass, the mass flux of the upflows,  $j_z^{\uparrow}$ , equals the mass flux of the downflows,  $j_z^{\downarrow}$ ) with

$$\nabla_{j_z} = \frac{\partial_z \ln |\langle j_z^{\uparrow\downarrow} \rangle|}{\partial_z \ln \langle p_{\text{th}} \rangle},$$

which indicates the length, over which the up- or downflow has changed by the  $e$ -fold, where the length scale is expressed in pressure scale heights. Trampedach & Stein (2011) introduced the mass mixing length as the inverse vertical mass flux scale height, i.e.  $l_m = \partial_z \ln |\langle j_z^{\uparrow\downarrow} \rangle|^{-1}$ , which is in concordance with the gradient of the vertical mass flux with  $l_m = H_P / \nabla_{j_z}$ . Furthermore, we define the mass mixing length as the inverse gradient of the vertical mass flux,

$$\alpha_m \equiv \nabla_{j_z}^{-1},$$

and we can decompose the gradient of the vertical mass flux into its components and find

$$\alpha_m = (\nabla_{\rho} + \nabla_{v_z})^{-1},$$

which states that the mass mixing length is the inverse sum of the changes in the density and vertical velocity gradients. We note that this definition is the same as introduced by Trampedach & Stein (2011). Finally, we can identify now the mass mixing length in the denominator of the vertical velocity (Eq. 1) and get the following expression

$$\langle v_z \rangle = \sqrt{\frac{\alpha_m}{1 + \alpha_m \nabla_{v_z}} \left( \frac{g}{\partial_z \ln \langle p_{\text{th}} \rangle} - \frac{\langle p_{\text{th}} \rangle}{\langle \rho \rangle} \right)}.$$
 (2)

This illustrates why the vertical velocity depends on the mass mixing length, similar to the MLT velocity  $v_{\text{MLT}}$  that depends on mixing length parameter with  $v_{\text{MLT}} \propto \alpha_{\text{MLT}}$  (see Eq. C.2).

To complete the comparison of the mass mixing length with the (MLT) mixing length parameter, we derive its dependence with the convective energy flux. The mean convective energy flux consists of the fluctuations of the total energy ( $\epsilon_{\text{tot}} = \epsilon + p_{\text{th}}/\rho + \mathbf{v}^2/2$ ), which we depicted with  $f$ , and is carried by the mean vertical mass flux, i.e.

$$\langle F_{\text{conv}} \rangle = \langle f \rangle \langle \rho v_z \rangle,$$

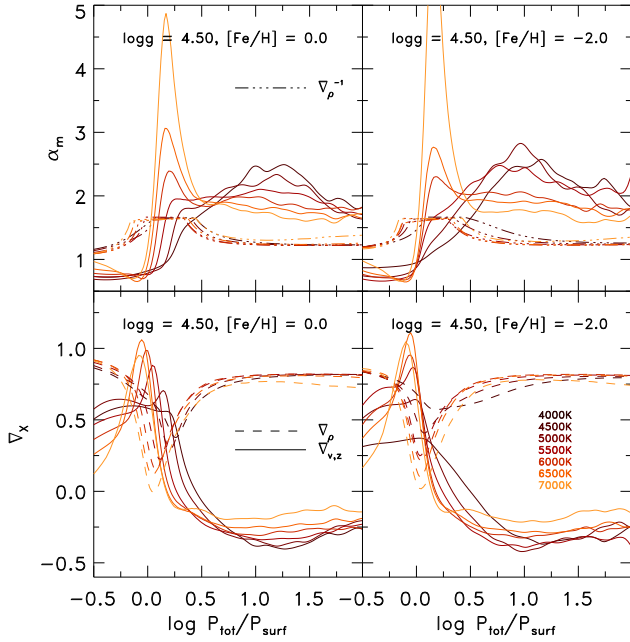


**Fig. 11.** *Top panel:* The mass mixing length  $\alpha_m$  (solid) and the inverse gradient of the density,  $\nabla_\rho^{-1}$  (triple-dotted dashed line). For clarity we excluded values with  $\nabla_\rho^{-1} > 5/3$  just below the optical surface ( $0 < \log p_{\text{tot}}/p_{\text{surf}} < 0.5$ ). *Bottom panel:* the gradient for density,  $\nabla_\rho$ , and vertical velocity,  $\nabla_{v_z}$ , (dashed and solid lines, respectively) for different stellar parameters.

where we assume that  $v_z$  is the hydrodynamic velocity given in Eq. 1. We determine the divergence of the convective energy flux, i.e.  $\partial_z \langle F_{\text{conv}} \rangle$ , and solve for the total energy fluctuations and get

$$f = \frac{1}{\nabla_\rho + \nabla_{v_z}} \frac{\partial_z \langle F_{\text{conv}} \rangle / \langle \rho v_z \rangle + \partial_z \langle f \rangle}{\partial_z \ln \langle p_{\text{th}} \rangle}.$$

Then, we can substitute the convective energy losses,  $\partial_z \langle F_{\text{conv}} \rangle$ , with the radiative cooling rate,  $-\langle q_{\text{rad}} \rangle$ , due to conservation of total energy, and we can identify the mass mixing length in the convective energy flux as well and yield

$$\langle F_{\text{conv}} \rangle = -\alpha_m \frac{(\langle q_{\text{rad}} \rangle + \langle \rho v_z \rangle \partial_z \langle f \rangle)}{\partial_z \ln \langle p_{\text{th}} \rangle}. \quad (3)$$

This equation is basically the expression for the conservation of energy. Both of these equations for the velocity and the convective energy flux are just reformulations of the hydrodynamic mean field equations. To close this set of equations one still would need information about the gradient of the velocity and total energy fluctuation, as well as the radiative cooling rates.

#### 4.2. Depth-dependence of the mass mixing length

In Fig. 11, we illustrate the horizontally and temporally averaged, depth-dependent mass mixing length for different stellar parameters, which we have derived from our 3D RHD simulations. In the convection zone, the mass mixing length has values around  $\sim 2$ , while above the optical surface,  $\alpha_m$  exhibits lower values around  $\sim 0.5$ . Fuhrmann et al. (1993) found that similar low values for the mixing length parameter  $\alpha_{\text{MLT}}$  yield better fits for Balmer lines, however, they also use large values for the temperature distribution parameter with  $y = 0.5$  (see also App. C.2),

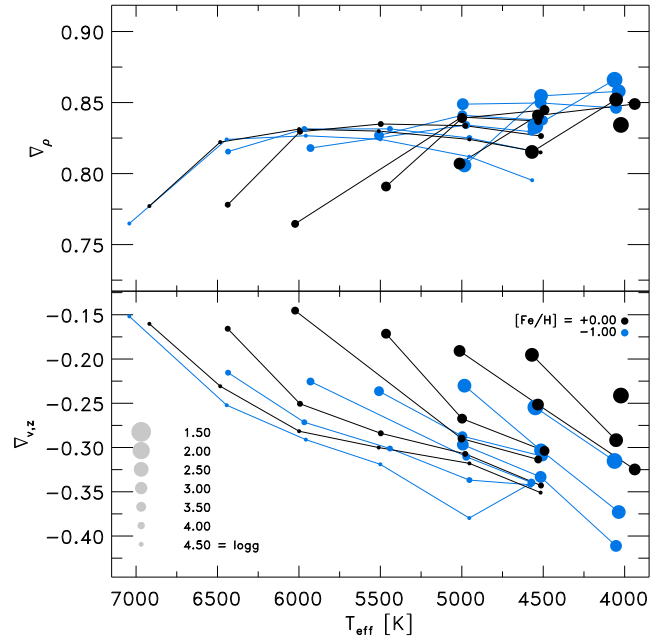


**Fig. 14.** The mean gradient of the density,  $\nabla_\rho$ , and the vertical velocity,  $\nabla_{v_z}$ , in the convection zone for different stellar parameters.

and also the influence of  $\alpha_{\text{MLT}}$  becomes negligible towards the optical surface, where the Balmer lines form (see Fig. 1). Therefore, the agreement of the depth-dependent  $\alpha_m$  with their low values for  $\alpha_{\text{MLT}}$  might be just a coincidence. Furthermore, just below the optical surface ( $\log p_{\text{tot}}/p_{\text{surf}} = 0$ ) at the photospheric transition region,  $\alpha_m$  features a peak, which depends on the stellar parameters, in particular, for higher  $T_{\text{eff}}$ , the peak in between increases, while in the convection zone it is the flatter. We remark that the peak in  $\alpha_m$  coincides with the location of the peak in the  $v_{z,\text{rms}}$ . We included also the inverse gradient of density in the same figure with  $\alpha_m$ , demonstrating that the adiabatic value of  $\alpha_m$  in the convection zone is mainly contributed by the density gradient.

We show also the gradients of the density and vertical velocity in Fig. 11, which are the both components of  $\alpha_m$ . One can depict that the variation of  $\alpha_m$  in the convection zone arises mainly due the different velocity gradients, since the density gradient converges always against very similar adiabatic values ( $\gamma_{\text{ad}} \simeq \nabla_\rho^{-1}$ ). For a monoatomic ideal gas with radiation pressure the adiabatic exponent is given by  $\gamma_{\text{ad}} = (1 - \nabla_{\text{ad}})^{-1}$ , and with  $\nabla_{\text{ad}} = 1/4$  one gets  $\gamma_{\text{ad}} \sim 4/3$  (Kippenhahn et al. 2013, see). When one considers  $\nabla_\rho^{-1}$  (see Fig. 11), it is close to 1.2. For a non-ideal gas differences due to non-ideal effects are to be expected. On the other hand,  $\nabla_\rho$  is close to  $\sim 0.8$ , therefore, similar to a value for an ideal gas with  $3/4$ , while  $\nabla_{v_z}$  is between  $-0.4$  and  $-0.15$  (see also Fig. 14).

At the vicinity of the optical surface, the cooling rates are imprinted in the gradients for the density and velocity with a sharp transition. Towards the interior, the density is increasing due to the stratification and hydrostatic equilibrium, hence the gradient is  $\nabla_\rho > 0$ , while the velocity is decreasing, and therefore  $\nabla_{v_z} < 0$ . The signs of  $\nabla_\rho$  and  $\nabla_{v_z}$  are opposite due to the conservation of mass. In the interior, the stellar fluid gets compressed, and the velocity slows down, i.e. the convective energy is carried with slower, thicker mass flux. For higher  $T_{\text{eff}}$ , the (negative) velocity gradient has a lower amplitude and therefore closer to zero, and

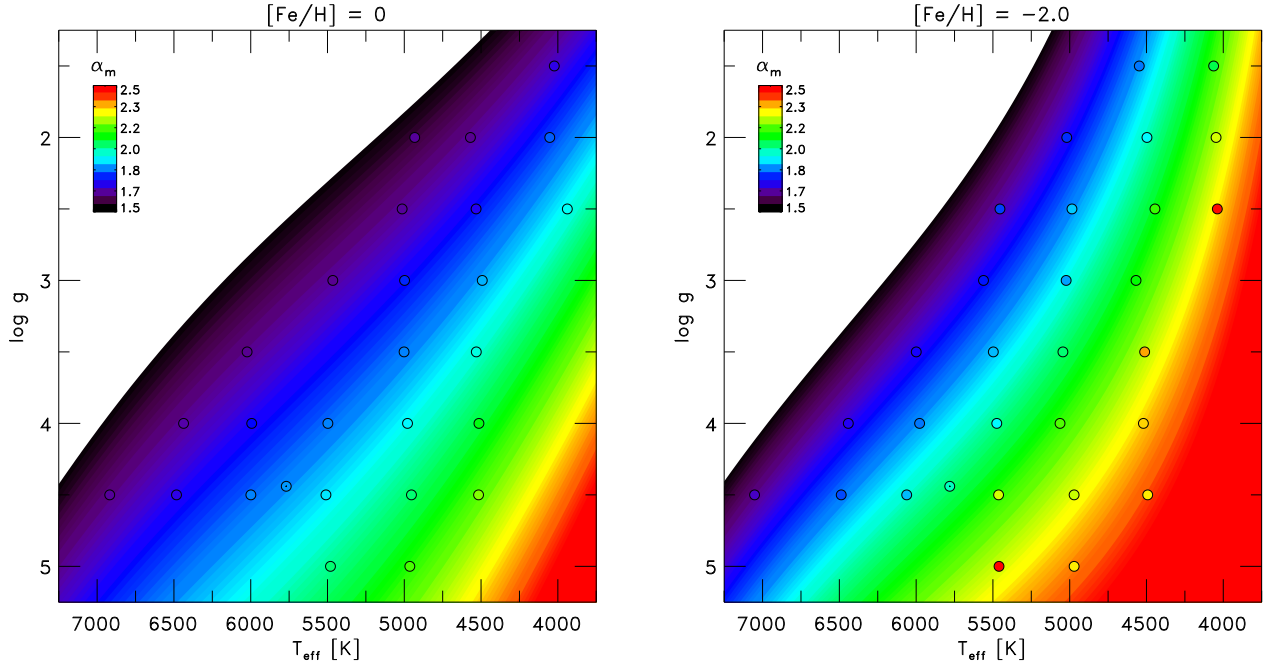


**Fig. 12.** As Fig. 2, but here the mass mixing length  $\alpha_m$  is shown.

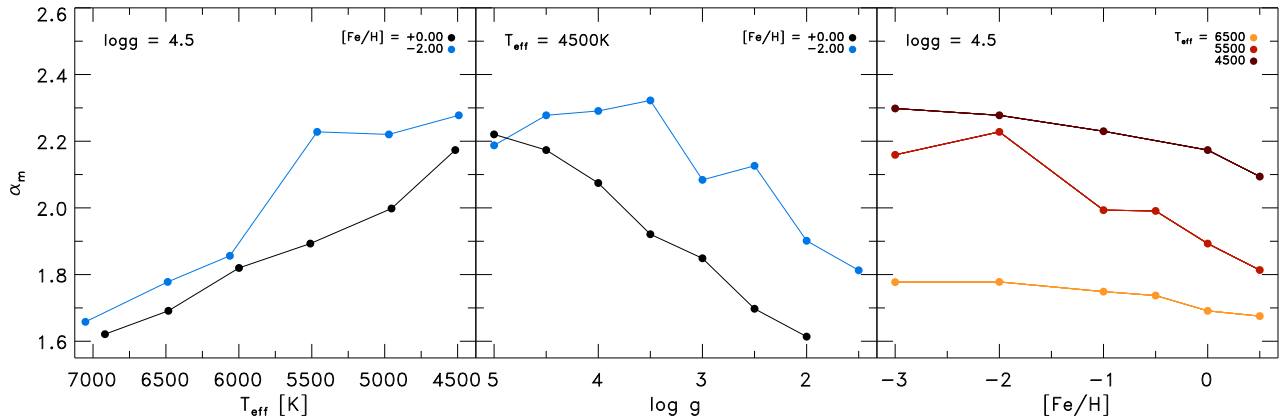


**Fig. 13.** As Fig. 4, but here the mass mixing length  $\alpha_m$  is shown.

a smaller amplitude of  $\nabla_{v_z}$  implies a steeper drop of the vertical velocity towards the interior, which also entails a larger maximum of the vertical velocity (see Fig. 14). The velocity gradient is reducing the density gradient, however, a lower sum of  $\nabla_\rho$  and  $\nabla_{v_z}$  relates to a higher  $\alpha_m$  due to the inverse relation (see Fig. 12). Since the density gradient is very similar for different stellar parameters, the variation in  $\alpha_m$  arises mainly from the differences in the velocity gradient, therefore, we can relate the variation of the entropy jump with the variation of the velocity gradient, i.e.  $\Delta s \sim e^{\nabla_{v_z}}$ , which was also concluded by Trampedach & Stein (2011) for the mass mixing length in an extended solar simulation.

#### 4.3. Mean mass mixing length in the convection zone

We determined the *mean* mass mixing length of the convection zone below the optical surface between the location of the peak in the density scale height, i.e.  $\max(\partial_z \ln \rho)_{\tau>1}$ , and the bottom, however, avoiding bottom boundary effects on the vertical velocity. We performed linear fits of the density and vertical rms-

velocity gradients by considering all snapshots, and from both gradients we determined the mean value of  $\alpha_m$ . The convection zones in the 3D simulations have to be extended enough, so that lower boundary effects on the vertical velocities are minimized, which is the case for most models, except some metal-poor giants that are slightly too shallow for matching  $\alpha_m$  properly.

The results for  $\alpha_m$  are displayed in Fig. 12, while in Fig. 14 we depict the mean values of the density and velocity gradients. From the solar simulation we determined  $\alpha_m^\odot = 1.83$ , which is close to the solar mass mixing length by Trampedach & Stein (2011) with 1.76. Furthermore, the mass mixing length depicts qualitatively very similar systematic variations with stellar parameter, as we found for  $\alpha_{MLT}$  above. In particular, it decreases for higher  $T_{\text{eff}}$  and  $[\text{Fe}/\text{H}]$ , and lower  $\log g$ , and the range in  $\alpha_m$  between  $\sim 1.7$  and  $\sim 2.3$  is qualitatively similar to the that of  $\alpha_{MLT}$  (see also Fig. 13). In general, we find qualitatively similar values for  $\alpha_m$  as found by Trampedach & Stein (2011), in particular, the dwarf models ( $\log g = 4.5$ ) have a similar slope with  $T_{\text{eff}}$ .

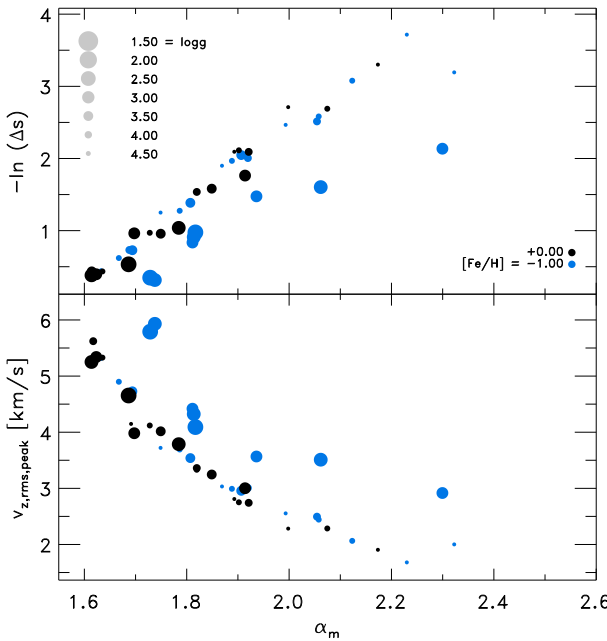


**Fig. 15.** Correlation of the mass mixing length,  $\alpha_m$ , with the logarithmic inverse of the entropy jump  $-\ln(\Delta s)$  and the peak of the vertical rms-velocity (top and bottom panel, respectively).

The variation of  $\alpha_m$  is also similar to the logarithmic inverse variation of the entropy jump. In Fig. 15 we compare  $\alpha_m$  with the logarithmic inverse entropy jump, and we find a similar tight correlation between the two, as we have found for the mixing length parameter  $\alpha_{\text{MLT}}(\Delta s)$  above (Sect. 3.3). The stronger deviations for the metal-poor giants originate from the fact that these models are slightly shallower, therefore, the match of the mass mixing length is perturbed due to the lower boundary effects on the velocity. We illustrate also the tight anti-correlation of the peak vertical rms-velocity with the mass mixing length in Fig. 15.

A comparison of the mass mixing length with the mixing length parameter calibrated with the entropy of the deep adiabatic convection zone and the entropy jump is shown in Fig. 16, and these correlate also well. The mixing length parameters are slightly higher than  $\alpha_m$  with a systematic offset around  $\sim 0.1$  and  $\sim 0.2$ , which is in the case of  $\alpha_{\text{MLT}}(s_{\text{bot}})$  smaller than for  $\alpha_{\text{MLT}}(\Delta s)$ . This illustrates that the mixing length parameter in the framework of MLT has a physical background rooted in the mass mixing length (or inverse vertical mass flux gradient). However, since the MLT is incomplete a one-to-one correspondence between  $\alpha_{\text{MLT}}$  and  $\alpha_m$  would be hardly to be expected, nonetheless, the good agreement between the two is an interesting result.

## 5. Velocity correlation length

The physical interpretation of the mixing length parameter is conceptually the mean free path of a convective eddy, over which it can preserve its identity, before it resolves into its environment. In a real stratified hydrodynamic fluid the spatial two-point (auto)correlation function of the vertical velocity can be regarded as the 3D analog of the mixing length parameter  $\alpha_{\text{MLT}}$  as proposed by Chan & Sofia (1987). The two-point correlation

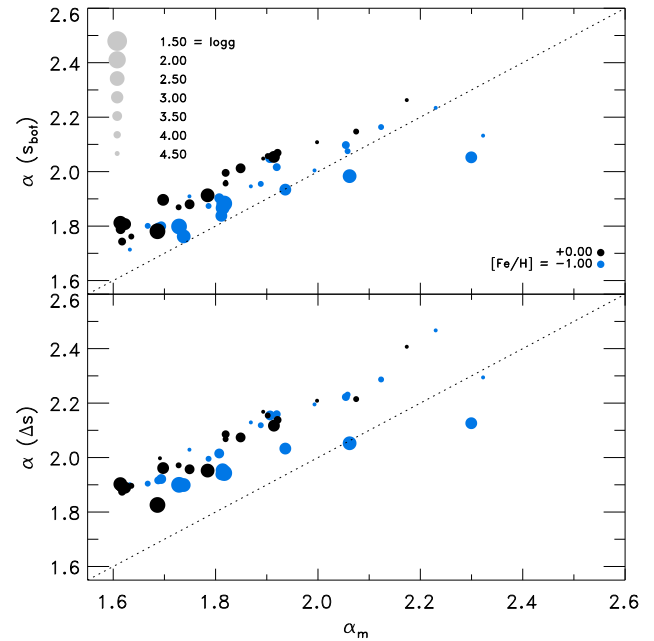


**Fig. 16.** Comparison of the mass mixing length,  $\alpha_m$ , with the mixing length parameter calibrated with  $s_{\text{bot}}$  and  $\Delta s$  (top and bottom panel, respectively).

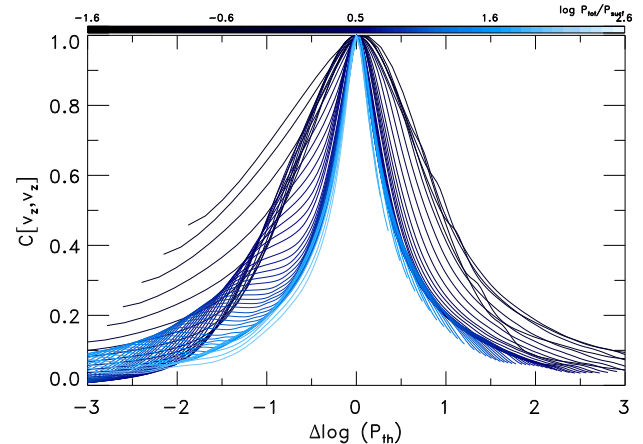


**Fig. 17.** Vertical two-point correlation function of the vertical velocity,  $C[v_z, v_z]$ , vs. the difference in the thermodynamic pressure,  $\Delta \log(P_{\text{th}})$ , for the solar simulation. The different heights are indicated with a blue color-coding. Note the convergence of the correlation width in the convection zone against an adiabatic value.

function for the values  $q_1$  and  $q_2$  is given by

$$C[q_1, q_2] = \frac{\langle q_1 q_2 \rangle - \langle q_1 \rangle \langle q_2 \rangle}{\sigma_1 \sigma_2}, \quad (4)$$

with  $\sigma_i$  being the standard deviation of  $q_i$  and  $\langle \dots \rangle$  depicts the spatial horizontal average. To derive the vertical correlation function of the convective velocity field, we consider the vertical component of the velocity field,  $v_z$ , of a single fixed layer  $z_0$  and derived the correlation functions for all other layers  $z_i$ , i.e.  $C[v_{z_0}, v_{z_i}]$ , which is performed for twenty equidistant layers covering the whole vertical depth scale of the simulation box.

In Fig. 17 we show the two-point correlation function of the vertical velocity field,  $C[v_z, v_z]$ , derived for the solar simulation for the individual snapshots and then temporally av-

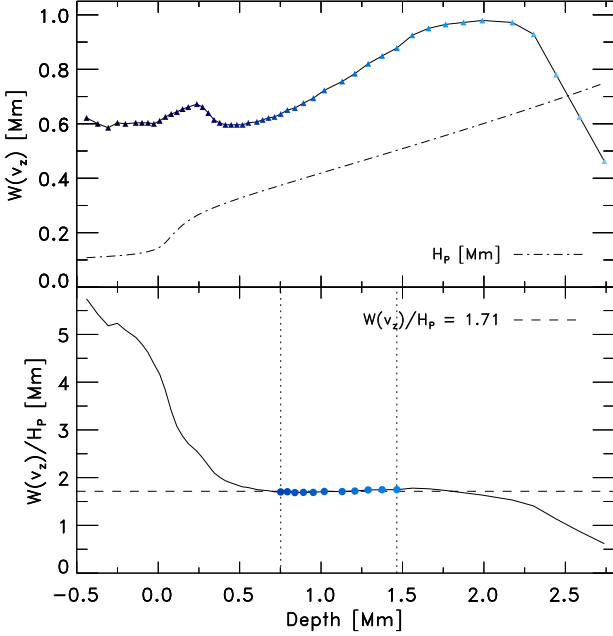


**Fig. 18.** *Top panel:* Vertical correlation length of the vertical velocity (solid line with triangles) and pressure scale height (dotted-dashed line) shown against the depth for the solar model. We indicated the different heights with the same color-coding as used in Fig. 17. *Bottom panel:* Vertical correlation length scaled by the pressure scale height, which yields an average of 1.71 (dashed line) in the considered region for averaging the correlation length (vertical dotted lines with filled circles) for the solar simulation.

eraged. For convenience, the correlation function is shown in differences of logarithmic pressure to the considered layer,  $\Delta \log P_{\text{th}} = \log P_{\text{th}}(z_0) - \log P_{\text{th}}(z_i)$ . Then, the correlation function reaches always unity for  $z_i = z_0$  and exhibits a Gaussian-like shape. Furthermore, it is broader above the optical surface ( $p_{\text{tot}}/p_{\text{surf}} = 1$ ), which is due to the rapid decline of the pressure scale height; while below the latter the width seems to converge against a certain adiabatic value (see Fig. 18). When one considers the width of the correlation function in geometrical depth, instead of pressure, then  $W(v_z)$  is constant around  $\sim 0.6 \text{ Mm}$  from the top down to  $\sim 0.5 \text{ Mm}$  and increases then with a fixed multiple (1.71) of the pressure scale height (see Fig. 18), which is the same as Robinson et al. (2003) found. The larger values for  $W(v_z)/H_P$  above 0.5 Mm result from the lower  $H_P$ .

The full-width-half-maximum (FWHM) of the two-point correlation function of the vertical velocity,  $C[v_z, v_z]$ , which we denote with  $W(v_z)$ , gives an estimate on the size or length scale of the coherent vertical structures. The characteristic local length scale for the turbulent convective eddies can be determined with  $W(v_z)$ . With the term vertical correlation length we refer to  $W(v_z)$ . Similar to the mixing length, it is preferable to scale the correlation length by the pressure scale height, i.e.  $W(v_z)/H_P$ , since the latter is increasing towards deeper layers. Then, for the solar simulation (see Fig. 18) the convergent value for the width is  $W(v_z)/H_P = 1.71$ . This means that the coherent vertical structures are extending  $1.71 H_P$  in the convection zone, and this value is comparable to the mixing length parameter ( $\alpha_{\text{MLT}} = 1.94$ ). Chan & Sofia (1987, 1989) found also a similar scaling of  $C[v_z, v_z]$  with pressure scale height in a 3D simulation for the Sun. For different stellar parameters we find a rather similar convergence of the correlation length of the vertical velocity in the convection zone (see Fig. 19).

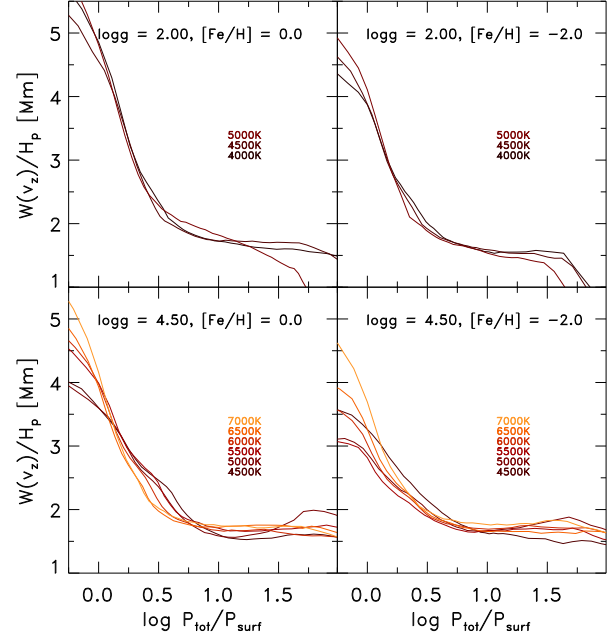


**Fig. 19.** Correlation length of the vertical velocity vs. surface normalized pressure for different stellar parameters.

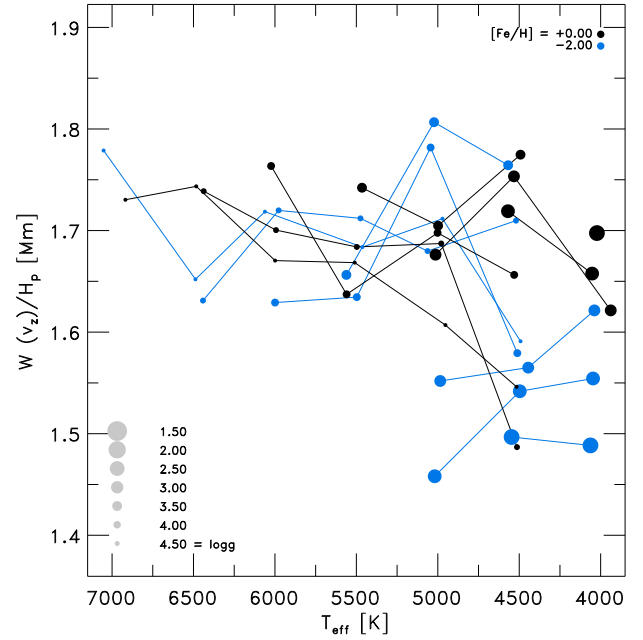


**Fig. 20.** Overview of mean vertical correlation length of the vertical velocity in the convection zone for different stellar parameters.

We determined also the mean value of correlation length in the convection zone below  $\log p_{\text{tot}}/\log p_{\text{surf}} > 1$  and close to the bottom boundary, the correlation function will increasingly overturn due to missing information in the deeper layers. Therefore, for the consideration of a mean correlation length we applied a cut at the bottom, where  $W(v_z)/H_P$  starts to turn towards lower values (see Fig. 18).

The resulting mean values of  $W(v_z)/H_P$  for different stellar parameters are depicted in Fig. 20, which are distributed between  $\sim 1.5$  and  $\sim 1.8$ . This is an interesting result, since it confirms, to a certain extent, the physical motivation for the mix-

ing length parameter,  $\alpha_{\text{MLT}}$ , namely the vertical velocity field, hence the vertical mass flux, correlates similarly with the pressure scale heights in the convection zone. However, the variation of  $W(v_z)/H_P$  with stellar parameters (Fig. 20) is not as clear and systematical, as we found above for  $\alpha_{\text{MLT}}$  and  $\alpha_m$  (see Sect. 4).

Furthermore, in contrast to the mixing length parameter ( $\alpha_{\text{MLT}}$  and  $\alpha_m$ ) the correlation length seems to increase for higher  $T_{\text{eff}}$ . The reason for this might be due to the horizontal granule size, which we found to decrease slightly for lower effective temperatures, since the pressure scale height is decreasing (see Paper I). Moreover, we find the granular cells, which can be highlighted with the temperature excess from the background, to feature distinct regular flat cylindric or pillar-like topologies.

Finally, we considered the correlation length of other variables, and we find that the horizontal velocity is rather similar, but with slightly lower correlation length with  $\sim 1.4$ . Also, we find for the entropy, temperature and pressure values around  $\sim 1.3$ , while for the density it is close to unity.

## 6. Conclusions

We have calibrated the mixing length parameter using realistic 3D RHD simulations of stellar surface convection by employing a 1D MLT stellar atmosphere code with identical micro-physics. The calibration was achieved by varying the mixing length parameter and matching the adiabatic entropy value of the deeper convection zone,  $s_{\text{bot}}$ , or alternatively matching the entropy jump,  $\Delta s$ . In both ways we find the mixing length to decrease for higher  $T_{\text{eff}}$  and  $[\text{Fe}/\text{H}]$ , and lower  $\log g$ . The mixing length varies in the range of  $1.7 - 2.3$  for  $\alpha_{\text{MLT}}(s_{\text{bot}})$  and  $\sim 1.8 - 2.4$  for  $\alpha_{\text{MLT}}(\Delta s)$ , and will lead to differences by up to  $\pm 20\%$  in  $\alpha_{\text{MLT}}$  depending on the stellar mass. This changes the stellar interior structure by extending or shortening the depth of the convection zone and thus the stellar evolution; we intend to return to how in detail a realistic  $\alpha_{\text{MLT}}$  will impact basic stellar evolution predictions in future studies.

Furthermore, we derived from the hydrodynamic mean field equations (for the first-time) a physical motivated connection of the mass mixing length, which is the inverse of the vertical mass flux gradient, with the mixing length. We determined the mass mixing length, and find that it varies qualitatively similar to the mixing length in the range of  $1.6 - 2.3$ . The mass mixing length exhibits also a depth-dependence and drops above the surface to lower values around  $\sim 0.5$ , which is in concordance to previous findings from observations. Finally, in both cases, the mass mixing length and mixing length, we find a strong correlation with the logarithmic inverse of the entropy jump for different stellar parameters, i.e.  $\alpha_{\text{MLT}} \sim -\ln \Delta s$ . Finally, we derived also the vertical velocity correlation length, which features similar values to the mixing length with approximately  $\sim 1.6 - 1.8$  of pressure scale height, however, the dependence with  $T_{\text{eff}}$  is inverted, i.e. the correlation length decreases with  $T_{\text{eff}}$ .

To summarize the importance of our work: we can finally remove the free parameters inherent in MLT and also avoid having to use solar calibrations for other stars.

**Acknowledgements.** We thank Regner Trampedach, Åke Nordlund and Bob Stein for helpful discussions. We acknowledge access to computing facilities at the Rechenzentrum Garching (RZG) of the Max Planck Society and at the Australian National Computational Infrastructure (NCI), where the 3D RHD simulations were carried out.

## References

- Asplund, M., Grevesse, N., Sauval, A. J., & Scott, P. 2009, ARA&A, 47, 481
- Böhm-Vitense, E. 1958, ZAp, 46, 108
- Bonaca, A., Tanner, J. D., Basu, S., et al. 2012, ApJ, 755, L12
- Canuto, V. M. 1989, A&A, 217, 333
- Canuto, V. M., Goldman, I., & Mazzitelli, I. 1996, ApJ, 473, 550
- Canuto, V. M. & Mazzitelli, I. 1991, ApJ, 370, 295
- Canuto, V. M. & Mazzitelli, I. 1992, ApJ, 389, 724
- Castelli, F. & Kurucz, R. L. 2004, ArXiv Astrophysics e-prints
- Chan, K. L. & Sofia, S. 1987, Science, 235, 465
- Chan, K. L. & Sofia, S. 1989, ApJ, 336, 1022
- Christensen-Dalsgaard, J. 2008, Ap&SS, 316, 13
- Deng, L., Xiong, D. R., & Chan, K. L. 2006, ApJ, 643, 426
- Freytag, B., Ludwig, H.-G., & Steffen, M. 1996, A&A, 313, 497
- Freytag, B., Ludwig, H.-G., & Steffen, M. 1999, 173, 225
- Freytag, B. & Salaris, M. 1999, ApJ, 513, L49
- Fuhrmann, K., Axer, M., & Gehren, T. 1993, A&A, 271, 451
- Gough, D. O. 1977, ApJ, 214, 196
- Grossman, S. A., Narayan, R., & Arnett, D. 1993, ApJ, 407, 284
- Gustafsson, B., Edvardsson, B., Eriksson, K., et al. 2008, A&A, 486, 951
- Henyey, L., Vardya, M. S., & Bodenheimer, P. 1965, ApJ, 142, 841
- Huber, D., Bedding, T. R., Stello, D., et al. 2011, ApJ, 743, 143
- Kippenhahn, R., Weigert, A., & Weiss, A. 2013, Stellar Structure and Evolution
- Kurucz, R. L. 1979, ApJS, 40, 1
- Ludwig, H.-G., Freytag, B., & Steffen, M. 1999, A&A, 346, 111
- Ludwig, H.-G., Jordan, S., & Steffen, M. 1994, A&A, 284, 105
- Magic, Z., Collet, R., Asplund, M., et al. 2013a, A&A, 557, A26
- Magic, Z., Collet, R., Hayek, W., & Asplund, M. 2013b, ArXiv e-prints
- Magic, Z., Serenelli, A., Weiss, A., & Chaboyer, B. 2010, ApJ, 718, 1378
- Mihalas, D. 1970
- Mihalas, D., Dappen, W., & Hummer, D. G. 1988, ApJ, 331, 815
- Nordlund, A. 1976, A&A, 50, 23
- Nordlund, A. 1982, A&A, 107, 1
- Nordlund, A. & Dravins, D. 1990, A&A, 228, 155
- Nordlund, Å., Stein, R. F., & Asplund, M. 2009, Living Reviews in Solar Physics, 6, 2
- Robinson, F. J., Demarque, P., Li, L. H., et al. 2003, MNRAS, 340, 923
- Schlattl, H., Weiss, A., & Ludwig, H.-G. 1997, A&A, 322, 646
- Steffen, M., Ludwig, H.-G., & Kruess, A. 1989, A&A, 213, 371
- Stein, R. F. & Nordlund, A. 1998, ApJ, 499, 914
- Trampedach, R. 2007, 948, 141
- Trampedach, R. & Stein, R. F. 2011, ApJ, 731, 78
- Unno, W., Kondo, M.-A., & Xiong, D.-R. 1985, PASJ, 37, 235
- Xiong, D. R., Cheng, Q. L., & Deng, L. 1997, ApJS, 108, 529

## Appendix A: Tables

In Table A.1, we have listed the results we have presented and discussed in this work. The complete table is available at CDS cdsarc.u-strasbg.fr and at www.stagger-stars.net as well.

## Appendix B: Functional fits

Similar to Ludwig et al. (1999), we performed functional fits of the mixing length parameters and the mass mixing length with the  $T_{\text{eff}}$  and  $\log g$  for the different metallicities individually. We transformed the stellar parameters with  $x = (T_{\text{eff}} - 5777)/1000$  and  $y = \log g - 4.44$ , and fitted the values with a least-squares minimization method for the functional basis

$$f(x, y) = a_0 + (a_1 + (a_3 + a_5 x + a_6 y)x + a_4 y)x + a_2 y. \quad (\text{B.1})$$

The resulting coefficients,  $a_i$ , are listed in Table B.1.

**Table A.1.** Stellar parameters: effective temperature,  $T_{\text{eff}}$ , and surface gravity,  $\log g$  (Cols. 1 and 2 in [K] and [dex]).

$T_{\text{eff}}$	$\log g$	$\lg \rho_{\text{bot}}$	$\lg T_{\text{bot}}$	$\lg p_{\text{th}}^{\text{bot}}$	$s_{\text{bot}}$	$\Delta s$	$\delta s_{\text{rms}}^{\text{peak}}$	$\delta \rho_{\text{rms}}^{\text{peak}}$	$v_{z,\text{rms}}^{\text{peak}}$	$\alpha_{\text{MLT}}^{s_{\text{bot}}}$	$\alpha_{\text{MLT}}^{\Delta s}$	$\alpha_m$	$W(v_z)/H_P$
4023	1.50	0.717	4.272	1.061	2.300	0.587	13.829	46.897	0.465	1.781	1.826	1.686	1.698
4052	2.00	1.125	4.233	1.368	2.018	0.354	8.885	35.288	0.379	1.913	1.952	1.784	1.658
3938	2.50	1.691	4.239	1.889	1.775	0.172	4.614	24.764	0.300	2.054	2.117	1.914	1.621
4569	2.00	0.679	4.342	1.120	2.411	0.683	15.947	50.583	0.525	1.812	1.903	1.614	1.719
4532	2.50	1.357	4.279	1.669	2.039	0.382	9.719	36.301	0.398	1.896	1.961	1.697	1.753
4492	3.00	1.785	4.266	2.029	1.808	0.206	5.636	26.808	0.325	2.012	2.074	1.849	1.775
4530	3.50	2.103	4.269	2.322	1.682	0.123	3.614	20.261	0.274	2.069	2.138	1.921	1.656
4513	4.00	2.419	4.277	2.625	1.578	0.068	2.154	14.454	0.229	2.147	2.215	2.075	1.487
4516	4.50	2.721	4.292	2.927	1.500	0.037	1.323	9.928	0.191	2.263	2.407	2.173	1.546
4512	5.00	3.013	4.308	3.226	1.434	0.020	0.817	6.377	0.154	2.345	2.875	2.221	1.684
5013	2.50	0.883	4.374	1.358	2.376	0.673	16.094	51.278	0.534	1.807	1.889	1.623	1.676
4998	3.00	1.534	4.308	1.882	2.024	0.384	9.898	35.942	0.402	1.880	1.957	1.749	1.705
5001	3.50	1.960	4.295	2.243	1.805	0.215	5.981	27.035	0.336	1.995	2.086	1.820	1.698
4978	4.00	2.292	4.293	2.538	1.661	0.121	3.605	19.745	0.275	2.057	2.155	1.902	1.687
4953	4.50	2.604	4.301	2.837	1.560	0.066	2.144	14.015	0.228	2.108	2.209	1.998	1.607
4963	5.00	2.885	4.314	3.118	1.485	0.038	1.370	9.888	0.185	2.143	2.228	2.130	1.577
5465	3.00	1.084	4.403	1.589	2.337	0.647	15.763	48.856	0.527	1.789	1.892	1.614	1.742
5560	3.50	1.663	4.345	2.062	2.040	0.410	10.655	37.436	0.418	1.861	1.951	0.000	1.637
5497	4.00	2.139	4.322	2.456	1.791	0.216	6.086	26.379	0.333	1.956	2.068	1.820	1.684
5510	4.50	2.486	4.322	2.769	1.649	0.123	3.690	19.527	0.281	2.048	2.168	1.893	1.668
5480	5.00	2.791	4.330	3.060	1.547	0.070	2.283	14.272	0.225	2.069	2.188	2.002	1.670
5768	4.44	2.367	4.336	2.688	1.725	0.179	5.171	23.788	0.308	1.982	2.090	1.825	1.702
6023	3.50	1.130	4.493	1.737	2.395	0.703	16.886	51.883	0.562	1.743	1.875	1.617	1.764
5993	4.00	1.865	4.364	2.281	1.991	0.379	10.084	35.917	0.412	1.869	1.971	1.728	1.700
5998	4.50	2.301	4.344	2.644	1.771	0.213	6.067	25.994	0.332	1.962	2.081	1.820	1.670
6437	4.00	1.384	4.495	1.989	2.315	0.647	15.974	48.227	0.533	1.762	1.896	1.635	1.739
6483	4.50	2.008	4.386	2.448	1.969	0.370	9.841	34.007	0.415	1.888	1.997	1.691	1.744
6918	4.50	1.545	4.543	2.201	2.292	0.640	15.600	46.039	0.526	1.792	1.908	1.621	1.730

Notes: The conditions at the lower boundary: density,  $\rho$ , temperature,  $T$ , pressure,  $p_{\text{th}}$ , entropy at the bottom; the entropy jump,  $\Delta s$ ; the peak fluctuations in: entropy,  $\delta s_{\text{rms}}^{\text{peak}}$ , density,  $\delta \rho_{\text{rms}}^{\text{peak}}$ , vertical velocity  $v_{z,\text{rms}}^{\text{peak}}$ ; the mixing length:  $\alpha_{\text{MLT}}(s_{\text{bot}})$  and  $\alpha_{\text{MLT}}(\Delta s)$ ; mass mixing length,  $\alpha_m$ , and correlation length  $W(v_z)/H_P$ .

## Appendix C: Addendum on MLT

### Appendix C.1: Mixing length formulation

In the framework of MLT, the convective flux is determined by

$$F_{\text{conv}} = [\alpha_{\text{MLT}} c_p T \Delta / 2] \rho v_{\text{MLT}}, \quad (\text{C.1})$$

with  $c_p$  being the heat capacity,  $\Delta$  the superadiabatic energy excess, and  $\alpha_{\text{MLT}}$  the adjustable *mixing length parameter*, giving the mean free path of convective elements in units of pressure scale height. The convective velocity is determined by

$$v_{\text{MLT}} = \sqrt{\alpha_{\text{MLT}}^2 g H_P \delta \Delta / \nu}, \quad (\text{C.2})$$

where  $H_P$  is the pressure scale height,  $\delta = -(\partial \ln \rho / \partial \ln T)_p$  the thermal expansion coefficient, and  $\nu$  the energy dissipation by turbulent viscosity. The superadiabatic excess is given by

$$\Delta = \frac{\Gamma}{(1 + \Gamma)} (\nabla - \nabla_{\text{ad}}), \quad (\text{C.3})$$

and the convective efficiency factor by

$$\Gamma = \frac{c_p}{8\sigma T^3} \tau_e (y + \tau_e^{-2}) \rho v_{\text{MLT}}, \quad (\text{C.4})$$

with the optical thickness  $\tau_e$ , and temperature distribution  $y$  of the convective element. The turbulent pressure

$$p_{\text{turb}} = \beta \rho v_{\text{turb}}^2, \quad (\text{C.5})$$

can be included, but a depth-independent turbulent velocity,  $v_{\text{turb}}$  is assumed, which is the common approach for atmospheric modeling. The resulting photospheric temperature stratifications are very similar to the MARCS (Gustafsson et al. 2008) and ATLAS models (Kurucz 1979; Castelli & Kurucz 2004). In Paper I, we showed that below the surface, where convective energy transport starts to dominate, the 1D models are systematically cooler than the 3D stratifications due to the fixed  $\alpha_{\text{MLT}}$  with 1.5, in particular for hotter  $T_{\text{eff}}$ .

### Appendix C.2: Influence of additional MLT parameters

In the Henyey et al. (1965) formulation of MLT, there are at least three additional free parameters apart from  $\alpha_{\text{MLT}}$ , which usually are not mentioned explicitly, but are compensated for by the value of  $\alpha_{\text{MLT}}$ . These are the scaling factor of the turbulent pressure,  $\beta$ , the energy dissipation by turbulent viscosity,  $\nu$ , and the temperature-distribution of a convective element,  $y$ . The default values are usually  $\beta = 1/2$ ,  $\nu = 8$  and  $y = 3/4\pi^2 = 0.076$  (see Gustafsson et al. 2008). In many cases the turbulent pressure is neglected ( $\beta = 0$ ). In the notation of Ludwig et al. (1999), these parameters would yield  $f_1 = \nu^{-1}$  and  $f_4 = y^{-1}$ ,  $f_2 = 1/2$  and  $f_3 = (8y)^{-1}$ .

The turbulent pressure indirectly influences the  $T$ -stratification, gradients and hydrostatic equilibrium by reducing the gas pressure. The parameter  $\nu$  enters the convective velocity inverse proportionally,  $v_{\text{MLT}} \propto \nu^{-1}$  (see Eq. C.2), and since  $v_{\text{MLT}} \propto \alpha_{\text{MLT}}^2$ , an increase in  $\nu$  would have the same effect as a

**Table B.1.** The coefficients  $a_i$  of the linear function  $f$  (Eq. B.1) for  $\alpha_{\text{MLT}}(s_{\text{bot}})$ ,  $\alpha_{\text{MLT}}(\Delta s)$ , and  $\alpha_m$  for different metallicities.

Value	[Fe/H]	$a_0$	$a_1$	$a_2$	$a_3$	$a_4$	$a_5$	$a_6$
$\alpha_{\text{MLT}}(s_{\text{bot}})$	+0.5	1.974688	-0.142021	0.170741	0.024297	0.052544	-0.022037	0.049356
	+0.0	1.977865	-0.106418	0.175735	-0.000828	0.119129	-0.063150	0.090105
	-0.5	1.957010	-0.134908	0.134950	0.029573	0.049614	-0.049488	0.060188
	-1.0	1.970111	-0.136446	0.148661	0.006539	0.060244	-0.047208	0.052210
	-2.0	2.010999	0.020070	0.159245	-0.022815	0.173832	-0.082277	0.088476
	-3.0	1.989143	0.047037	0.099284	-0.049489	0.125301	-0.066058	0.049417
	-4.0	2.105519	-0.026359	0.188547	-0.105125	0.210455	-0.027552	0.046338
$\alpha_{\text{MLT}}(\Delta s)$	+0.5	2.058149	-0.119213	0.180661	0.028582	0.085363	-0.024102	0.067584
	+0.0	2.089614	-0.091350	0.173393	-0.004769	0.102243	-0.068672	0.088211
	-0.5	2.089800	-0.115589	0.150432	0.067208	0.083192	-0.080297	0.117587
	-1.0	2.138877	-0.158683	0.203997	0.001463	0.099322	-0.032171	0.063329
	-2.0	2.228230	-0.101193	0.245259	-0.028850	0.188122	-0.075008	0.094004
	-3.0	2.230910	0.116557	0.216279	-0.114575	0.323863	-0.190753	0.150333
	-4.0	2.251819	-0.025839	0.223897	-0.161554	0.224572	-0.021968	-0.014593
$\alpha_m$	+0.5	1.794271	-0.185369	0.184148	-0.024718	0.099181	-0.026372	0.052865
	+0.0	1.834453	-0.187970	0.174615	0.013326	-0.006504	-0.022975	0.012212
	-0.5	1.875566	-0.260200	0.173911	0.110922	-0.038815	-0.058444	0.069665
	-1.0	1.962526	-0.421215	0.255133	0.016063	-0.127566	0.088774	-0.124965
	-2.0	2.018201	-0.282156	0.250964	-0.013607	0.042364	-0.016666	-0.013242
	-3.0	1.940639	-0.323805	0.191152	0.059047	-0.029973	0.013051	-0.045249

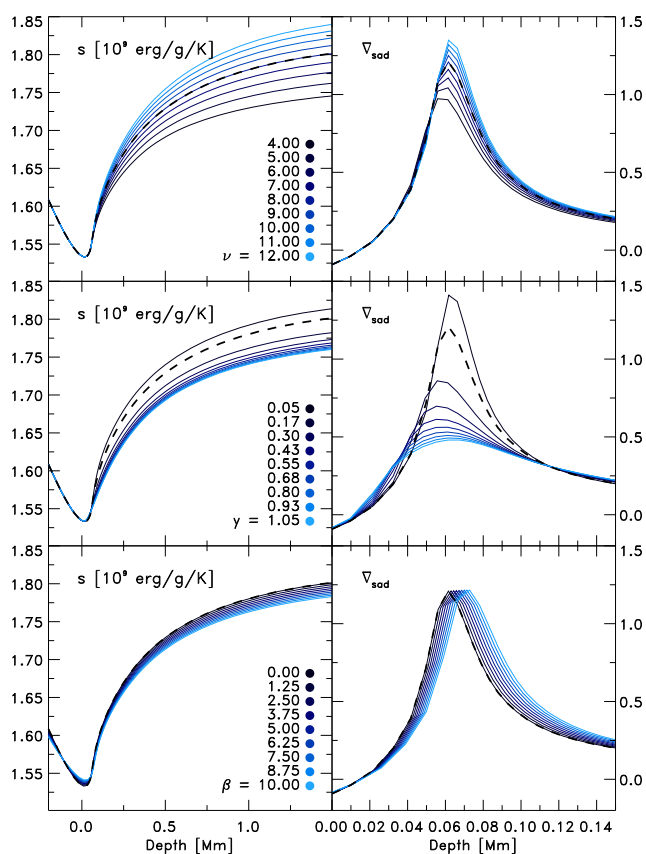


**Fig. C.1.** The entropy and superadiabatic gradient vs. depth (left and right panel, respectively) illustrating the influence of the additional MLT parameters  $v$ ,  $y$  and  $\beta$  (top, middle and bottom panel, respectively), the latter with the depth-independent  $v_{\text{turb}} = 1 \text{ km/s}$ . The mixing length is kept fixed at  $\alpha_{\text{MLT}} = 1.5$ . We included also the standard values of  $\beta = 0$ ,  $v = 8$  and  $y = 0.076$  (dashed lines). Shown is the case for solar parameters.

reduction in  $\alpha_{\text{MLT}}$ , i.e.  $v \propto s_{\text{bot}}$ . On the other hand,  $y$  enters in the (nonlinear) convective efficiency factor,  $\Gamma$ , for the superadiabatic excess (see Eq. C.4), and therefore  $y$  is correlated with  $\alpha_{\text{MLT}}$  in a more complex way.

Considering a variation of the three additional parameters in the computation of the solar 1D model, we notice that the adiabatic entropy value of the deep convection zone is altered significantly (see Fig. C.1). Furthermore, both parameters  $v$  and  $y$  also change the entropy jump and the superadiabatic temperature gradient,  $\nabla_{\text{sad}}$ , and in particular, its maximum of  $\nabla_{\text{sad}}$ . The effect of the variation of  $y$  on the entropy stratification is similar to that by  $\alpha_{\text{MLT}}$  (see Fig. 1). However, the entropy of the deep convection zone exhibits a more nonlinear dependence with the  $y$  parameter. The increasing turbulent pressure with higher  $\beta$  changes the stratification only slightly, but shifts the location of the maximum of  $\nabla_{\text{sad}}$  to the deeper interior. Towards the optical surface the influence of the MLT parameters is diminishing, as should be expected due to decreasing convective flux. A fine-tuning of  $\beta$ ,  $v$  and  $y$  is only useful, when these parameters introduce an independent influence to the mixing length, since otherwise its effects can be summarized in  $\alpha_{\text{MLT}}$  solely.